Multiphase patient-specific simulations to study fibrillation-induced thrombosis in the left atrial appendage

Anass Bouchnita, Vitaly Volpert, Nikolajus Kozulinas, Aleksey V Belyaev, Grigory Panasenko

▶ **To cite this version:**

Anass Bouchnita, Vitaly Volpert, Nikolajus Kozulinas, Aleksey V Belyaev, Grigory Panasenko. Multiphase patient-specific simulations to study fibrillation-induced thrombosis in the left atrial appendage. Physics of Fluids, 2024, 36 (7), pp.071912. 10.1063/5.0216196 . hal-04794334

HAL Id: hal-04794334
https://hal.science/hal-04794334v1

Submitted on 20 Nov 2024

HAL is a multi-disciplinary open access archive for the deposit and dissemination of scientific research documents, whether they are published or not. The documents may come from teaching and research institutions in France or abroad, or from public or private research centers.

L'archive ouverte pluridisciplinaire **HAL**, est destinée au dépôt et à la diffusion de documents scientifiques de niveau recherche, publiés ou non, émanant des établissements d'enseignement et de recherche français ou étrangers, des laboratoires publics ou privés.

AIP Publishing Physics of Fluids ACCEPTED MANUSCRIPT
This is the author's peer reviewed, accepted manuscript. However, the online version of record will be different from this version once it has been copyedited and typeset.
PLEASE CITE THIS ARTICLE AS DOI: 10.1063/5.0216196

Multiphase patient-specific simulations to study fibrillation-induced thrombosis in the left atrium appendage

Anass Bouchnita,[1] Vitaly Volpert,[2,3] Nikolajus Kozulinas,[4] Aleksey V. Belyaev,[5] and Grigory Panasenko[6]
[1)]*Department of Mathematical Sciences, The University of Texas at El Paso, El Paso 79902, Texas, USA*
[2)]*Institut Camille Jordan, UMR 5208 CNRS, University Lyon 1, 69622 Villeurbanne, France*
[3)]*Peoples Friendship University of Russia (RUDN University), 6 Miklukho-Maklaya St, Moscow, 117198, Russian Federation*
[4)]*Institute of Applied Mathematics, Vilnius University, Naugarduko Str., 24, Vilnius, 03225 Lithuania*
[5)]*M.V. Lomonosov Moscow State University, Faculty of Physics, 119991 Moscow, Russia*
[6)]*Institute of Applied Mathematics, Vilnius University, Naugarduko Str., 24, Vilnius, 03225 Lithuania*

(*Electronic mail: abouchnita@utep.edu)

(Dated: 26 June 2024)

Thrombosis commonly develops in the left atrial appendage of patients with atrial fibrillation. The formation of blood clots in atrial appendage is a complex process, which depends on the shape of the appendage, the velocity of blood flow, the concentrations of red blood cells, platelets, and coagulation, among other factors. In this work, we present a new methodology to identify the key factors contributing to clot formation in the left atrial appendage during atrial fibrillation. The new methodology combines computed tomography imaging, computational fluid dynamics, mesh processing, and multiphase thrombosis modeling. We begin by running simulations to investigate flow patterns inside the left atrial appendages with realistic geometries. Our simulations suggest that at the entrance of the left atrial appendage the flow forms vortices, which can intrude inside the appendage depending on the phases of the cardiac cycle. Next, we introduce blood coagulation and consider different scenarios corresponding to physiological values of blood flow velocity, geometry of the left atrial appendage, and hematocrit values. Numerical results suggest that the chances of clot formation are higher in the "cactus" geometry than in the "chicken-wing" one, in agreement with the literature. Furthermore, they suggest that slower flow circulation facilitates the development of a clot in the depth of the left atrial appendage. Slower blood movement also favors the procoagulant activity of platelets, while faster flow circulation enhances the procoagulant effect from erythrocytes. Finally, our simulations show that increased hematocrit upregulates the generation of fibrin polymer, regardless of flow velocity.

Keywords: mixture theory, computer-aided decision system, atrial fibrillation, blood coagulation

I. INTRODUCTION

About 50% of ischemic strokes have cardioembolic origin[1,2]. Atrial fibrillation (AF) is one of the most frequent causes of thrombosis and stroke, and in the case of nonvalvular AF more than 90% of thrombi are localized in the left atrium appendage (LAA)[3]. The LAA is a muscular sac connected by a lumen (orifice) to the left atrium through the ostium and is part of the normal anatomy of the human heart. Its anatomy and biomechanical properties make it suitable to function as a decompression chamber during left ventricular systole when left atrial pressure is high[4]. The onset of LAA thrombosis can be identified in clinical practice by a spontaneous echo contrast observed during transoesophageal echocardiography, and it is usually related to a decrease of inflow and outflow velocities at the orifice of the appendage[4]. Therefore, depressed LAA biomechanical function (contractility), which is typical for AF, may result in thrombus formation. The size and mobility of such thrombi are considered to be the main determinants of thromboembolic risk[5].

Great risks in patients with atrial fibrillation are related to the formation of floating intracardiac thrombi, which may interfere with cardiovascular functions in many ways, leading to thromboembolism, transient ischemic attack[6], fatal or disabling stroke[7]. A lot of attention and effort is devoted to this problem nowadays, as modern methods of prediction and treatment of thrombosis are constantly evolving: from conventional diagnostics[8,9] to patient-specific predictive computational fluid dynamics (CFD) modeling for risk estimation[10–13] and deep-learning approaches[14]; from preventive anticoagulant[15,16] to a resolute choice between surgery[17] and implantable devices[7,18–20] bearing the consequent risk of device-related thrombosis[21] and a need for anti-platelet therapy[22,23]. Another study identified a correlation between the higher incidence rate of LAA occlusion and low hypoattenuation thickening during the use of devices[24]. Understanding of biophysical mechanisms underlying LAA thrombosis is an important step in predicting the dynamics of the adverse cardiovascular events caused by blood clotting, which, in turn, is crucial for determining the therapy strategy.

In Ref.[25], the LAA thrombi are classified as membranous M-thrombi and polypoid-shape P-thrombi. M-thrombi are observed in the majority of AF patients. They are flat and they are formed by a fibrin layer covered later by endothelial cells, they do not contain platelets or RBC. M-thrombi are fragile and can rupture due to hydrodynamic (or other) forces. P-thrombi appear in the sites of rupture of M-thrombi. P-thrombi contain red blood cells, platelets and fibrin, they resemble red thrombi in blood vessels. Thrombi can form either in the tip or near the orifice of LAA depending on the pathology or their combination (AF, mitral stenosis). The

AIP Publishing Physics of Fluids ACCEPTED MANUSCRIPT
This is the author's peer reviewed, accepted manuscript. However, the online version of record will be different from this version once it has been copyedited and typeset.
PLEASE CITE THIS ARTICLE AS DOI: 10.1063/5.0216196

correlation between LAA morphology and thromboembolism risks are underlined by prior clinical studies[26,27], thus eliciting important roles of hemodynamics[28,29], blood rheology[10] and spontaneous aggregation of blood cells[30–34]. The biophysical reasons for some of the involved phenomena are still being debated[30,34].

Blood clots may appear due to multiple factors including endothelial dysfunctions, blood stasis, inflammation, increased concentrations of coagulation factors in the blood, etc.[35]. The exact mechanistic picture of thrombogenesis in LAA is still unclear.

Two principal components of hemostasis and thrombosis are the blood platelets that aggregate in response to biochemical signaling or hydrodynamic forces, and the blood plasma clotting (coagulation), i.e., polymerization of the fibrin protein as a result of a cascade of enzymatic reactions[36–39]. These branches are apparently coupled and support each other providing positive and negative feedback loops[40–42]. It also seems that fluid mechanics plays a leading role in the regulation of thrombus size and growth rate in blood vessels of various geometries[36,43–46]. However, the hydrodynamic conditions may drastically vary through the circulatory system, resulting in distinctive dynamics of thrombus growth and the composition of clots formed in arteries[38,47–49], arterioles and microvasculature[37] from those in veins[50,51], aneurysms and re-circulation zones[52,53].

Platelet adhesion and activation from binding to collagen, damaged or inflamed endothelium, or from soluble biochemical agonists is one of the main processes of initial arterial and microvascular hemostasis, where the shear stress in fluid is relatively high[37,38,47–49,54]. Several recent studies also mention the manifold role of red blood cells (RBC) in triggering and supporting thrombosis and hemostasis: from mechanical and rheological effects[55–59] to biochemical response, aggregation and involvement into cellular signaling[60–63]. The coagulation of plasma may be triggered apart from platelet aggregation through either the extrinsic or the intrinsic pathway[39,64], however, it is inhibited by fluid motion and manifests in stagnant areas[44] or inside the aggregates[37].

The concept of Virchow's triad proposes that thrombosis is the result of abnormal blood flows, vascular endothelial injury, or alterations in the presence of coagulation factors in plasma. The first and the second points are particularly relevant for relatively slow flows inside the LAA even in patients without coagulation disorders. While damaged or inflamed endothelium is considered to be the most evident trigger of the LAA thrombosis[65,66], the hemodynamic conditions itself may provoke vascular inflammation or damage[67,68]. At the same time, the phenomenon of spontaneous echo contrast in LAA[4], which is strongly associated with the onset of thrombosis, thromboembolism, and adverse cerebrovascular events, may indicate that the blood cells accumulated in the slow flow regions activate their adhesive and signaling functions and aggregate thus influencing the permeability of the atrial appendage to the blood flow and promoting the clotting[30,31].

By summarizing and uniting known mechanisms of hemostasis into one computational framework, we proposed a general model of LAA thrombosis that includes hemostatic reactions and fluid dynamics. Hence, it integrates all mechanical peculiarities, rheology, and blood cell interactions, inflammation of endothelium of the LAA walls, platelet adhesion, and activation, and the cascade of plasma coagulation[52,69–71]. The present study is focused on a patient-specific approach to biomedical engineering, therefore, special procedures are proposed to unify all the stages of simulations. The multiscale nature of the problem is challenging and thus requires intelligent approaches[72].

Several accurate computational fluid dynamics (CFD) simulations are found in literature[13,73–75] proposing different ways to account for the realistic patient-specific geometry of the atrium and the appendage. Recent studies relate thrombosis risks to hemodynamics and blood rheology inside the LAA, underlining a protective role of active myocardium contractions that normally occur in sinus rhythm and are absent in AF case[10,74–76]. Some unconventional approaches employ deep-learning and AI techniques for an acceleration of thrombosis risk estimation based on LAA geometry[14]. However, these works mostly inspect the streamlines, fluid velocity, and wall shear stress, predicting the endothelial cell damage or activation, yet thrombus dynamics in usually excluded from the analysis. Recently a 2D model of a thrombus growing in LAA has been considered in Ref.[11] by using Navier-Stokes equations for the blood flow and three equations for the concentration of blood factor (thrombin, fibrinogen, fibrin). The computational domain corresponded to the left atrium with periodically oscillating boundaries and different geometries of LAA. The initiation of blood coagulation occurs at the LAA wall in one of three chosen areas near the orifice, in the middle, and in the tip. In agreement with clinical observations, numerical simulations show that the risk of clot growth is lower for LAA with chicken-wing morphology and higher for broccoli. The risk of clot formation increases in the case of atrial fibrillation modeled as decreased wall motion. The transport and aggregation of cellular and molecular species in biofluids is an important problem studied by CFD[77–79].

In the present study, we focus on two particular LAA geometries ("chicken wing" and "cactus") that are frequently found in patients with AF. We model blood flow in a fully patient-specific left atrium using COMSOL[80] for a heart pulsation cycle. We then use this data to validate the multiphase model describing thrombus growth in the left atrial appendage over longer time scales. The multiphase model is implemented using the OpenFOAM library[81] and uses an idealized geometry for the left atrium, except for the patient-specific shape of the left atrial appendage. Our goal is to compare the thrombus growth dynamics for these cases and thus inspect a possible correlation between the LAA geometry and risks of thrombotic events. The continuum description of the hemostatic response system (partial differential equations) provides high scalability and versatility of our model. We overcome the limitations of prior studies by including the validated model of plasma coagulation[45,82,83] and complement it with previously validated CFD methods[52,56,84,85] for explicit accounting of the interplay between intracardial hemodynamics and thrombogenesis.

The manuscript is organized as follows. In the Model and

AIP Publishing Physics of Fluids ACCEPTED MANUSCRIPT
This is the author's peer reviewed, accepted manuscript. However, the online version of record will be different from this version once it has been copyedited and typeset.
PLEASE CITE THIS ARTICLE AS DOI: 10.1063/5.0216196

Methods section, we provide the mathematical description and present the assumptions underlying the equations. We also describe the techniques that allowed linking the patient-specific clinical data on geometry and hemodynamics, domain decomposition, CFD, and the mathematical model of thrombus growth. Next, in the Results section we present the simulation data obtained with the presented model. In the Discussion section, we analyze the results of the present work and outline future directions of studies and ways of improvement of existing CFD approaches for modeling LAA thrombosis. Then, we present the Conclusion section.

II. METHODS

A. General concept of the approach

Let us describe the numerical setup, Fig.1. It consists of two stages. In the first stage, we solve numerically the Navier-Stokes equations for the blood (one phase model) in the real-life patient-specific geometry obtained from the computed tomography images (CT) of the left atrium (LA) including the left atrial appendage (LAA). The geometry of the domain is obtained via imaging and cleaning procedures using the SOLIDWORKS software[86]. The meshing procedure provides a fine mesh. Patient-specific flow velocity at the pulmonary veins was measured and used for validation purposes. Measurements were made for 16 seconds, corresponding to 20 cardiac cycles of 0.8 seconds. As flow velocity during the first 6 seconds was not yet established, then only the results for the last 10 seconds were considered. In this study we consider average blood velocity shown on Fig. 1 and prescribe it on each of four pulmonary veins. Similar boundary conditions for velocity were then implemented on all four pulmonary veins. The high-accuracy computations give the velocity field of the blood in LA.

Then, the model of the thrombogenesis is solved in a domain with simplified idealized geometry of the LA but with the original geometry of LAA. Idealized left atrium geometries were previously used to analyze the factors contributing to the development of thrombosis in the LAA using sensitivity analysis[87]. To construct this domain, we extract the patient-specific LAA geometry and simplify it using MeshLab[88]. Then, we incorporate this part into an idealized geometry of the LA that we constructed using the CAD software Salome-Meca[89]. This approach allows us to accelerate the computations of the thrombogenesis in LAA, reducing the mesh in the main part of the LA. The boundary conditions of the inflow to LAA are validated by the values of velocity computed by the Navier-Stokes model in three points of the LAA. Two types of LAA morphology are considered: the “chicken wing” and the “cactus”, Fig.2. The idealized left atrium has a length of 8 cm and an internal radius of 3.5 cm. It has four inlets of 1.25 cm diameter and one outlet of 3 cm diameter. The location of the LAA is chosen to mimic its position in the patient-specific LA. The Meshlab utility was used to simplify the inlet boundary region of the LAA to allow it to be merged with the idealized LA. The SnappyHexMesh utility was used to generate the mesh under the OpenFOAM library[90]. The generated meshes consist of 13,937 and 14,601 hexahedra for the chicken wing and the cactus cases, respectively. All simulations were carried out in 3D. The CPU time for simulations with the multi-phase model is approximately 10-12 minutes for 200 seconds of the physical time on a i6 laptop with 16 GB of ram.

B. Patient-specific LAA morphology and blood flow

The objective of this work is to study the dynamics of clot growth in different LAA patient-specific geometries and coagulation settings. Therefore, we consider an idealized geometry for all the left atrium, except the LAA which is taken from the computed tomography images of real patients. The obtained geometry has four inlets, corresponding to the four pulmonary veins, and one outlet representing the mitral valve (Figure 2). The locations of the LAA inlet is considered to be the same in the two settings. Each LAA has thrombogenic surfaces where tissue factor is produced and coagulation can be initiated. The location and size of these thrombogenic surfaces is chosen to mimic clinical observations[91].

To study clot growth in realistic hemodynamic conditions that correspond to atrial fibrillation (AF), we correlate inlet flow to measured electrocardiogram doppler measurement of an AF patient. Next, we use the CFD package COMSOL[80], to simulate flow dynamics inside the left atrium of a patient during a period of ten seconds. We use the obtained results to calibrate the inlet of the multiphase model, such that the simulated flow intensity in three points approximate the one observed in the CFD simulations. To achieve this, we have gradually increased the flow intensity at the LA inlet until the simulated flow velocity at the LAA entrance matches the one estimated using the CFD package. The objective is not to have accurate reproduction of the flow dynamics, but to make sure that the flow intensity approximates the one computed in the patient-specific geometry. The obtained results shown in Fig. 3 suggest a relatively good agreement in terms of flow magnitude and peak timings between the multi-phase model that used the idealized left atrium geometry and the CFD model that considers the patient-specific morphology.

In the paper we consider two scenarios of the thrombus formation corresponding to different velocity magnitudes at the entrance of the LAA. This approach is motivated by an uncertainty of the experimental data on the velocity: the measurement is provided in the zone where the velocity changes drastically. Numerical computations show that by moving the point of measurement from "a bit inside" the LAA to “a bit outside” LAA the velocity increases several times. In Fig. 4 we sketch a “cut line” through the left atrium passing from the dorsal part of the LAA to the opposite wall of the left atrium. Along this line we obtain the following values for the euclidean norm of the velocity in m/s at $t = 1.9$ s. The figure shows how drastically changes the velocity near the entrance to the LAA. That is why the experimental data are very sensitive to the point of measurement which is not always exactly placed in the experiment. Also, the velocity direction at the entrance of the LAA plays an important role. In particular, in

ACCEPTED MANUSCRIPT
Physics of Fluids
AIP Publishing
This is the author's peer reviewed, accepted manuscript. However, the online version of record will be different from this version once it has been copyedited and typeset.
PLEASE CITE THIS ARTICLE AS DOI: 10.1063/5.0216196

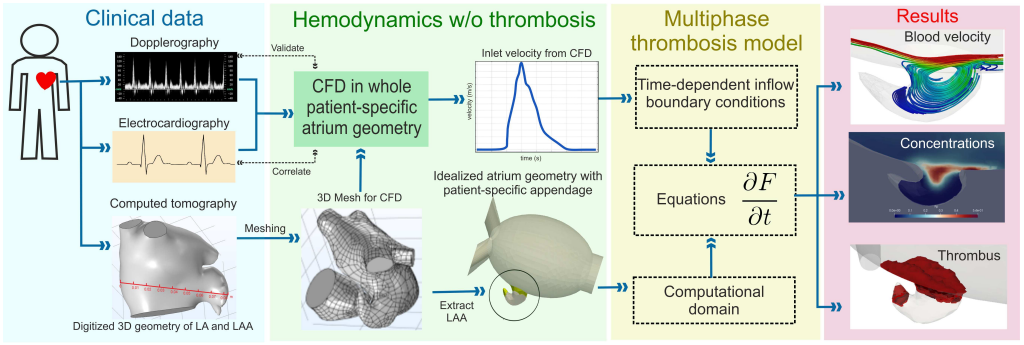

FIG. 1. A flowchart representing the general concept of the proposed patient-specific approach.

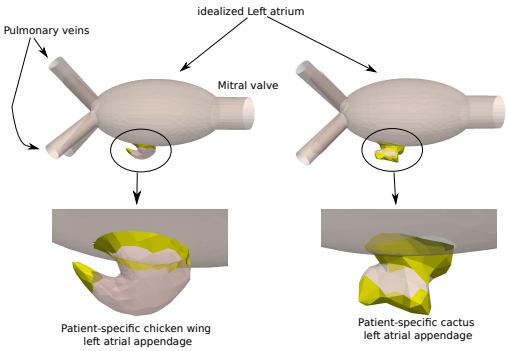

FIG. 2. Geometry of the two domains where clot growth is simulated, corresponding to an idealized left atrium with a chicken wing (left) and cactus (right) LAA morphologies. An idealized geometry for the left atrium is considered for all patients. It consists of four pulmonary veins representing the inlet and a mitral valve corresponding to the outlet. The left atrial appendage is taken from patient-specific images. Yellow surfaces correspond to thrombogenic surfaces where clot growth is initiated.

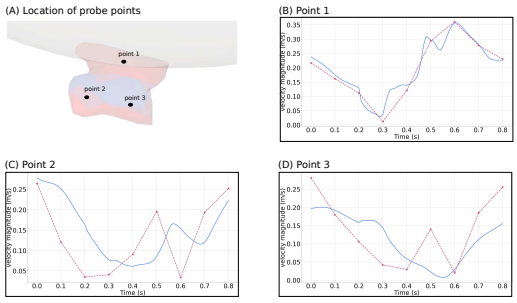

FIG. 3. A comparison between the magnitude of flow velocity at three points inside the left atrium appendage simulated from simulations using the multi-phase model (dark pink) and the CFD for the patient-specific geometry (blue). The inlet flow velocity in the multi-phase model was calibrated such that the intensity of flow inside the LAA mimics the one simulated using the CFD model.

Ref.[75] the dominating tangential direction of the velocity with respect to the plane of the entrance to the LAA is pointed out in the case of the fibrillation. In this case the normal component may be very small. Further, it was shown that the geometry of the LAA influences the magnitude and patterns of flow observed inside the LAA[92].

C. Computational model for thrombosis

We introduce a continuum model to describe the spontaneous formation of blood clots in stagnant and low-flow regions. The proposed approach conceptually includes three main parts: fluid dynamics, interaction and activation of blood cells, and plasma coagulation, as summarized in Fig. 5. The blood is represented by a two-phase fluid, which motion is described by a multi-component model. The model captures the dynamics of platelet deposition, activation and aggregation, as well as their interactions with RBCs, by using a continuous approach. Here also we consider a previously developed model of the coagulation cascade[45,82] which consists of the following concentration fields: prothrombin P, thrombin T, antithrombin A, fibrinogen F_g, fibrin F, fibrin polymer F_p. Thrombin - the main activator of fibrin polymerization - is produced from prothrombin due to a sequence of biochemical processes. The detailed mathematical formulation of the computational model for thrombosis in stagnation and flow recirculation zones can be found in Ref.[52] together with validation results. Appendix A summarizes all the cellular, chemical and physical variables involved in the model.

ACCEPTED MANUSCRIPT
Physics of Fluids
AIP Publishing
This is the author's peer reviewed, accepted manuscript. However, the online version of record will be different from this version once it has been copyedited and typeset.
PLEASE CITE THIS ARTICLE AS DOI: 10.1063/5.0216196

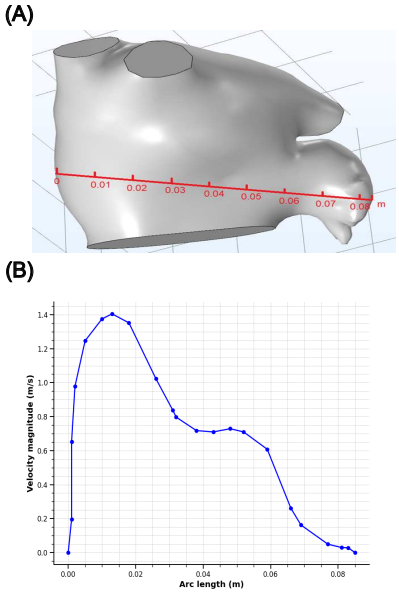

FIG. 4. (A) The "cut line" across the atrium considered to evaluate flow velocity. (B) The calculated euclidean norm of the flow velocity along the "cut line".

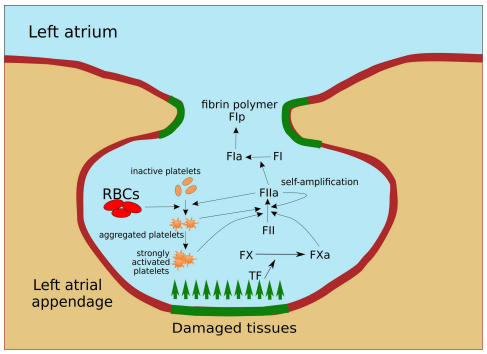

FIG. 5. A schematic representation of the thrombus formation process implemented in the present model. The left atrial appendage is an extension originating from the main volume of the left atrium: the inner volume filled with blood is depicted here with the cyan color, and the non-fluid tissue (myocardium) is colored in sienna. Our multiphase thrombosis model considers several pathways of plasma coagulation and accounts for a two-stage aggregation and activation of blood platelets. The role of RBCs in promoting platelet aggregation and thrombosis is versatile: it includes rheology and mechanics, as well as biochemical signaling.

1. *Hemodynamics and blood rheology in the model*

We apply a previously developed and validated multicomponent model for hemodynamics[52,56]. Fluid equations are solved using OpenFOAM 6.0[81] with the Pressure Implicit with Splitting of Operators (PISO) method[93]. The approach of the model consists in employing the mixture theory to depict blood flow as a two-phase fluid, representing blood plasma and red blood cells separately:

$$\rho_p\left(\frac{\partial \mathbf{v}_p}{\partial t}+(\mathbf{v}_p\cdot\nabla)\mathbf{v}_p\right)=\nabla\cdot\mathbf{T}_p+\rho_p\mathbf{b}_p+\mathbf{f}_I-\mathbf{f}_b^p, \quad (1)$$

$$\rho_s\left(\frac{\partial \mathbf{v}_s}{\partial t}+(\mathbf{v}_s\cdot\nabla)\mathbf{v}_s\right)=\nabla\cdot\mathbf{T}_s+\rho_s\mathbf{b}_s-\mathbf{f}_I-\mathbf{f}_b^s. \quad (2)$$

Here, $\mathbf{T}_p$ and $\mathbf{T}_s$ denote Cauchy stress tensors for plasma and RBCs, while $\mathbf{b}_p$ and $\mathbf{b}_s$ are body forces; $\mathbf{f}_I$ describes a body force for interaction between the phases[56], and $\mathbf{f}_b^p$ and $\mathbf{f}_b^s$ account for flow deceleration upon encountering a clot. The two-way coupling between plasma and RBCs is symmetrically integrated into the right-hand sides of Eqs.(1) and (2). Plasma is modelled as a Newtonian fluid, while RBCs follow a non-Newtonian rheology.The velocity is computed as $\mathbf{v}=(1-\phi)\mathbf{v}_p+\phi\mathbf{v}_s$, with ϕ determined by hematocrit, reflecting the RBC fraction. We also define the local shear rate in the fluid (mixture) $\dot{\gamma}$ as follows:

$$\dot{\gamma}=(2\,\mathrm{Tr}\,\mathbf{D}^2)^{1/2}, \quad (3)$$

where $\mathbf{D}=\frac{1}{2}[\nabla\mathbf{v}+(\nabla\mathbf{v})^T]$ is the strain rate tensor of the fluid, and "Tr" corresponds to the trace of a tensor. Mass conservation equations are given for each phase as follows:

$$\frac{\partial \rho_p}{\partial t}+\nabla\cdot(\rho_p\mathbf{v}_p)=0, \quad \frac{\partial \rho_s}{\partial t}+\nabla\cdot(\rho_s\mathbf{v}_s)=0. \quad (4)$$

Here ρ_p and ρ_s represents the density of the plasma and RBC phases, respectively. They depend on the pure (constant) densities of the plasma and RBCs phases and the RBC volume fraction as follows:

$$\rho_s=\rho_{s0}\phi, \quad \rho_p=\rho_{p0}(1-\phi). \quad (5)$$

The evolution of the RBC volume fraction can be tracked using the following equation:

$$\frac{\partial \phi}{\partial t}+\nabla\cdot(\mathbf{v}_s\phi)=0, \quad (6)$$

derived from RBC density equations and $\rho_s=\rho_{s0}\phi$. We proceed to establish mass conservation for the entire fluid. We deduce the equation for volume fraction $(1-\phi)$ using the plasma phase density equation and $\rho_p=(1-\phi)\rho_{p0}$. After simplification with positive constant ρ_{p0}, we arrive at:

$$\frac{\partial (1-\phi)}{\partial t}+\nabla\cdot(\mathbf{v}_p(1-\phi))=0. \quad (7)$$

AIP Publishing Physics of Fluids ACCEPTED MANUSCRIPT
This is the author's peer reviewed, accepted manuscript. However, the online version of record will be different from this version once it has been copyedited and typeset.
PLEASE CITE THIS ARTICLE AS DOI: 10.1063/5.0216196

We sum the equations (6) and (7), and we take $\phi + (1-\phi) = 1$, which gives us:

$$\nabla \cdot \mathbf{v} = 0, \tag{8}$$

where $\mathbf{v} = \phi \mathbf{v_s} + (\mathbf{1} - \phi)\mathbf{v_p}$, is the velocity of the whole fluid. Overall, we numerically solve the Equations (1), (2), (6), and (8) to determine the changes in RBCs velocity ($\mathbf{v_s}$), plasma velocity ($\mathbf{v_p}$), RBC volume fraction ϕ, and fluid pressure p.

Tensors and interaction forces for each phase are adopted from a prior study[56]. This study assumes the plasma to exhibit Newtonian rheology, leading to the following expression for its stress tensor:

$$\mathbf{T}_p = [-p(1-\phi) + \lambda_p(1-\phi)\,\mathrm{Tr}\mathbf{D}_p]\mathbf{I} + 2\mu_p(1-\phi)\mathbf{D}_p, \tag{9}$$

where p is the pressure of the flow, λ_p and μ_p are first and second coefficient of plasma viscosity, $\mathbf{D}_p = \frac{1}{2}\left[(\nabla \mathbf{v}_p) + (\nabla \mathbf{v}_p)^T\right]$, "Tr" represents the trace of a tensor, $\mathbf{I}$ is the identity tensor.

For the RBCs phase, non-linear fluid rheology is assumed and the stress tensor is given by:

$$\mathbf{T}_s = \left[-p\phi + \beta_{20}(\phi + \phi^2)\,\mathrm{Tr}\mathbf{D}_s\right]\mathbf{I} + \mu_s(\phi, \dot{\gamma}_s)\phi\mathbf{D}_s, \tag{10}$$

and we adopt a Cross-Power Law model for the rheology of RBCs:

$$mu_s(\phi, \dot{\gamma}_s) = \mu_\infty(\phi) + [\mu_0(\phi) - \mu_\infty(\phi)]\frac{1}{1 + m\dot{\gamma}_s} \tag{11}$$

$$\dot{\gamma}_s = (2\,\mathrm{Tr}\mathbf{D}_s^2)^{1/2}. \tag{12}$$

Here, the effect of hematocrit on the viscosity of RBCs is captured using the following correlations[56]:

$$\mu_0(\phi) = 537.002\phi^3 + 55.006\phi^2 - 0.129\phi, \tag{13}$$

$$\mu_\infty(\phi) = 27.873\phi^3 - 21.218\phi^2 + 14.439\phi. \tag{14}$$

The interaction forces ($\mathbf{f}_I$) between two components of the mixture (plasma and RBCs) describe the Stokes drag and the phenomenological expression for the near-wall shear-induced lift force on[56]:

$$\mathbf{f}_I = \frac{9\mu_p}{2a^2}\phi[\exp(2.68\phi) + \phi^{0.43}](\mathbf{v}_s - \mathbf{v}_p) + \frac{3 \cdot 6.46 \cdot (\rho_p \mu_p)^{1/2}}{4\pi a}\phi(2\,\mathrm{Tr}\mathbf{D}_p^2)^{-1/4}\mathbf{D}_p(\mathbf{v}_s - \mathbf{v}_p),$$

where $a = 8\ \mu$m is the diameter of a red blood cell.

Flow deceleration within the clot is considered as well. To capture the clot's impact on hemodynamics, we model the thrombus as a porous medium. The hydraulic resistance hinges on active platelet and fibrin polymer concentrations. Viscous friction in blood crossing the clot is mathematically represented by force terms $\mathbf{f}_b^p$ and $\mathbf{f}_b^s$, expressed as:

$$\mathbf{f}_b^p = \frac{\mu_p}{K_f}\mathbf{v}_p, \quad \mathbf{f}_b^s = \frac{\mu_s}{K_f}\mathbf{v}_s, \tag{15}$$

where μ_p and μ_s are the plasma and RBCs phases viscosities, verifying $\mu = (1-\phi)\mu_p + \phi\mu_s$ is the blood viscosity and

$$\frac{1}{K_f} = \frac{16}{a_p^2}\bar{F_p}^{3/2}(1 + 56\bar{F_p}^3)\left(\frac{P_{c,max} + (P_c^1 + P_c^2)}{P_{c,max} - (P_c^1 + P_c^2)}\right), \tag{16}$$

where $\bar{F_p} = min(\frac{7}{10}, \frac{F_p}{7000})$, according to Ref.[94]. Boundary conditions for the velocities of the RBC and plasma phases, fluid pressure as well as the volume fraction of RBCs are given in Table I.

Field	Inlet	Outlet	Walls
$\mathbf{v_s}$	Dirichlet (equal to inlet velocity)	Zero-flux	No-slip
$\mathbf{v_p}$	Dirichlet (equal to inlet velocity)	Zero-flux	No-slip
p	Zero-flux	Dirichlet ($p = 0$)	Zero-flux
ϕ	Dirichlet ($\phi = 0.5$)	Zero-flux	Zero-flux

TABLE I. The boundary conditions used for the different fields considered in the hemodynamics model.

2. *Modeling platelet aggregation and activation*

In this model, platelets fall into three categories: a) mobile platelets (P_f) suspended in the fluid, moving with the flow; b) aggregated platelets (P_c^1) with active GPIIb/IIIa receptors, lending mechanical stability via fibrinogen-dependent binding[95]; c) highly activated platelets (P_c^2) expressing P-selectin[96], capable of activating aggregated platelets through granule secretion, ADP, and soluble agonists. While aggregated (P_c^1) and strongly activated (P_c^2) platelets correspond to the "shell" and "core" of observed microvascular thrombi[37], we avoid this notation due to potential differences in platelet localization in stagnation and recirculation zones. The equation for mobile platelets in the flow (P_f) reads:

$$\begin{aligned}\frac{\partial P_f}{\partial t} &+ \nabla \cdot (\mathbf{v}P_f) - \nabla \cdot \left[(D_B + \zeta\phi\dot{\gamma})\nabla(1 + q(\phi))P_f\right] \\ &- \nabla \cdot \left[(D_B + \zeta\phi\dot{\gamma})(1 + q(\phi))\nabla P_f\right] \\ &= -\frac{k_1 P_f}{1 + K_1 F_p}P_f - k_2 R P_f - \frac{k_3(P_c^1 + P_c^2)}{1 + K_1 F_p}P_f - k_4 T P_f.\end{aligned} \tag{17}$$

Here, the third and fourth terms in the left-hand side of this equation describe the diffusion of platelets in areas where the density of RBCs is low[56]. $D_b = 1.5810^{-13} m^2 s^{-1}$ is the platelet diffusion coefficient and $\zeta = 6.010^{-14} m^{-2}$ is a constant, $q(\phi)$ is a polynomial function given by:

$$q(\phi) = 0.26\phi + 10.6\phi^2 + 537\phi^3. \tag{18}$$

The equation's right-hand side comprises:

- The first term denotes aggregation of mobile platelets via GPIb-VWF binding and subsequent GPIIb/IIIa activation through established mechano-transduction pathways[36,97]. At low shear rates ($< 1000\ s^{-1}$),

ACCEPTED MANUSCRIPT
Physics of Fluids
AIP Publishing
This is the author's peer reviewed, accepted manuscript. However, the online version of record will be different from this version once it has been copyedited and typeset.
PLEASE CITE THIS ARTICLE AS DOI: 10.1063/5.0216196

fibrinogen-mediated bonds between low-affinity GPIIb/IIIa receptors can lead to platelet aggregation, independent of GPIb-VWF[95]. The product $\frac{1}{1+K_1F_p}$ represents the reduction in platelet aggregation to the coverage of aggregated platelets by a fibrin cap[98].

- The second term accounts for platelet-RBC interaction through FasL/FasR complex formation[63], triggering GPIIb/IIIa activation and aggregation. Besides that, RBCs can bind platelets directly via αIIbβ3-ICAM4 molecular bonds[99] and activate platelets biochemically by releasing ATP and ADP under hypoxia or acidosis[62]. Here, R represents local normalized RBC concentration. It is obtained by multiplying the RBC phase fraction field (ϕ) by the considered hematocrit value.
- The third term signifies recruitment of platelets from flow by already aggregated (P_c^1) and activated (P_c^2) ones, implying activation of resting platelets by secreted ADP and agonists. Both aggregated and strongly activated platelets activate resting ones at the same rate.
- The last term models platelet activation by thrombin, stimulating protease-activated receptors (PAR) on the platelet membrane.

The initial and inlet platelet value is set to the physiological value of $P_{f0} = 300 \times 10^9 L^{-1}$, with zero-flux boundary conditions at other boundaries. Next, we describe the density of aggregated platelets (P_c^1):

$$\frac{\partial P_c^1}{\partial t} + \Psi(P_f + P_c^1 + P_c^2)\nabla\cdot(\mathbf{v}P_c^1 - D_p\nabla P_c^1) = \frac{k_1 P_f}{1+K_1F_p}P_f + k_2 R P_f + \frac{k_3(P_c^1+P_c^2)}{1+K_1F_p}P_f + k_4 T P_f - k_5\dot{\gamma}P_c^1 - k_6 P_c^1. \quad (19)$$

Here, the motility of platelets hinges on their overall concentration, described by $\Psi(P_f + P_c^1 + P_c^2) = \tanh(\phi(1 - \frac{P_f+P_c^1+P_c^2}{P^{max}}))^{42}$. The term $-k_5\dot{\gamma}P_c^1$ accounts for removal of loosely connected platelets due to shear stress, while the final term $-k_6 P_c^1$ signifies strong platelet activation, intensifying their adhesion. We consider that removed platelets cannot attach again to the clot. Finally, the strongly activated platelets (P_c^2) are described as follows:

$$\frac{\partial P_c^2}{\partial t} = k_6 P_c^1 - k_7\dot{\gamma}P_c^2. \quad (20)$$

The final term represents platelet detachment by flow. Here, k_7 is chosen such that $k_7 \ll k_5$ due to stronger attachment of highly activated platelets, resulting from increased adhesiveness, density, and clot contraction[37,100]. This assumption mirrors the biological observation that strongly activated platelets bind more tightly to the thrombus. However, we also account for the removal of these strongly activated platelets. Zero-flux conditions are applied to aggregated platelets (P_c^1) and to strongly activated platelets (P_c^2) on all boundaries.

3. Coagulation cascade

We apply an existing model to depict coagulation cascade biochemistry in flow[45,82]. This model has been employed to elucidate thrombosis mechanisms in conditions like antithrombin deficiency[83] and rheumatoid arthritis[101]. Thrombin holds a pivotal role, converting fibrinogen to fibrin, constituting the cross-linked fibrin mesh upon polymerization. Thrombin generation from prothrombin is self-sustaining, driven by positive feedback involving platelets and cascade factors; antithrombin and similar factors counteract thrombin production. Here, we present the rationale for reducing the coagulation cascade equation system. Let us consider the following model describing the self-amplification of thrombin production[102]:

$$\frac{\partial [Va]}{\partial t} = \bar{k_1}T - h_1[Va], \quad (21)$$

$$\frac{\partial [VIIIa]}{\partial t} = \bar{k_2}T - h_2[VIIIa], \quad (22)$$

$$\frac{\partial [XIa]}{\partial t} = \bar{k_3}T - h_3[XIa], \quad (23)$$

$$\frac{\partial [IXa]}{\partial t} = \bar{k_4}[XIa] - h_4[IXa], \quad (24)$$

$$\frac{\partial [Xa]}{\partial t} = (\bar{k_5}[IXa] + \bar{k_{55}}[VIIIa][IXa])(U^0 - U) - h_5[Xa], \quad (25)$$

$$\frac{\partial T}{\partial t} = (\bar{k_6}U + \bar{k_{66}}U[Va])P - h_6 T. \quad (26)$$

Here, k_i signifies activation coefficient rates, while h_i represents inhibition rates. Va and Xa create the prothrombinase complex $Va-Xa$, and $VIIIa$ and IXa form $VIIIa-IXa$ complex. These are integrated into (25) and (26) via terms $k_{55}[VIIIa][IXa]$ and $k_{66}U[Va]$, assuming detailed equilibrium for large reaction constants. Additional equations for prothrombin, platelets, antithrombin, fibrinogen, fibrin, and fibrin polymer can be considered, but they do not impact thrombin production amplification. This allows independent study of the presented system. Detailed equilibrium assumption allows expressing coagulation factor concentrations as follows:

$$[Va] = \frac{\bar{k_1}}{h_1}T, \quad [VIIIa] = \frac{\bar{k_2}}{h_2}T, \quad [XIa] = \frac{\bar{k_3}}{h_3}T, \quad [IXa] = \frac{\bar{k_3}\bar{k_4}}{h_3 h_4}T, \quad (27)$$

$$[Xa] = \frac{\bar{k_3}\bar{k_4}}{h_3 h_4}T\left(\frac{\bar{k_5}}{h_5} + \frac{\bar{k_{55}}\bar{k_2}}{h_2 h_5}\right) \quad (28)$$

AIP Publishing Physics of Fluids ACCEPTED MANUSCRIPT
This is the author's peer reviewed, accepted manuscript. However, the online version of record will be different from this version once it has been copyedited and typeset.
PLEASE CITE THIS ARTICLE AS DOI: 10.1063/5.0216196

Substituting these concentrations with their expression in (25) and (26), we obtain:

$$\frac{\partial P}{\partial t} = -(K_8 T + K_9 T^2 + K_{10} T^3) P, \tag{29}$$

$$\frac{\partial T}{\partial t} = (K_8 T + K_9 T^2 + K_{10} T^3) P - h_6 T, \tag{30}$$

where

$$K_8 = \frac{\bar{k_3}\bar{k_4}\bar{k_5}\bar{k_6}}{h_3 h_4 h_5}, \quad K_9 = \frac{\bar{k_2}\bar{k_3}\bar{k_4}\bar{k_5}\bar{k_6}}{h_2 h_3 h_4 h_5} + \frac{\bar{k_1}\bar{k_3}\bar{k_4}\bar{k_5}\bar{k_6}}{h_1 h_3 h_4 h_5}, \tag{31}$$

$$K_{10} = \frac{\bar{k_1}\bar{k_2}\bar{k_3}\bar{k_4}\bar{k_5}\bar{k_6}}{h_1 h_2 h_3 h_4 h_5}, \tag{32}$$

and $h_6 = k_{11} A$. The reduced model gives a good approximation of the rate of clot growth described by the system (21) - (26)[103].

Subsequently, incorporating the procoagulant platelet types (P_c^1 and P_c^2), we establish equations for the spatiotemporal evolution of prothrombin, thrombin, and antithrombin concentrations in a simplified manner. The prothrombin equation is as follows:

$$\frac{\partial P}{\partial t} + \nabla \cdot (\mathbf{v} P - D_t \nabla P) = - \left[k_p (P_c^1 + P_c^2) + K_8 T + K_9 T^2 + K_{10} T^3 \right] P, \tag{33}$$

where the first term in the right-hand side of this equation represents the conversion of prothrombin by PS present on the surface of activated platelets, and the three other terms describe the kinetics of the amplification phase of the coagulation cascade. The concentration of thrombin is described by the following equation:

$$\frac{\partial T}{\partial t} + \nabla \cdot (\mathbf{v} T - D_t \nabla T) = \left[k_p (P_c^1 + P_c^2) + K_8 T + K_9 T^2 + K_{10} T^3 \right] P - K_{11} A T, \tag{34}$$

where the last term in the right-hand side of this equation describes the inhibition of thrombin by antithrombin. Prothrombin gets converted into thrombin as it gets close to inflammed tissues, due to the expression of tissue factor on these surfaces, which activates factors IX and X leading to the conversion of prothrombin into thrombin. We consider the following boundary conditions for prothrombin and thrombin on inflammed walls:

$$\frac{\partial P}{\partial \mathbf{n}} = -\frac{K_1 P}{D(1+\beta_1 P)}, \quad \frac{\partial T}{\partial \mathbf{n}} = \frac{K_1 P}{D(1+\beta_1 P)}. \tag{35}$$

The concentration of antithrombin is governed by the following equation:

$$\frac{\partial A}{\partial t} + \nabla \cdot (\mathbf{v} A - D_a \nabla A) = -K_{11} A T. \tag{36}$$

The remaining equations capture the kinetics of fibrinogen F_g, fibrin F, and fibrin polymer F_p concentrations:

$$\frac{\partial F_g}{\partial t} + \nabla \cdot (\mathbf{v} F_g - D_f \nabla F_g) = -K_{13} F_g T, \tag{37}$$

$$\frac{\partial F}{\partial t} + \nabla \cdot (\mathbf{v} F - D_f \nabla F) = K_{13} F_g T - K_{14} F, \tag{38}$$

$$\frac{\partial F_p}{\partial t} = K_{14} F. \tag{39}$$

The list of all variables described is provided in our previous work[52]. Parameter values for the multiphase blood flow model were adopted from a prior study[52,56], while those for coagulation cascade kinetics and fibrin clot formation were derived from another source[69]. It is a model for venous thrombosis that validated based on coagulation initiation microfluidics experiments[104], calibrated for thrombin generation dynamics in mice. Platelet subtype interactions with red blood cells were fine-tuned using experimental data for thrombus growth in a backward step geometry[52,105]. Appendix B summarizes the results obtained during the experimental validation of the model. Active protein (thrombin, T; fibrin, F) and fibrin polymer (F_p) species are governed by zero-flux boundaries. Initial and inlet zymogen (P, A, F_g) concentrations match blood physiology, and zero-flux boundaries apply to walls and the outlet. At the outlet, a zero-flux boundary condition is enforced for all species. Simulation codes are available from the corresponding author (A.B.) upon request.

D. Numerical and computational implementation of the coagulation model

The coagulation model solver was implemented under the OpenFoam library[81]. The choice of the numerical schemes and the mesh was made to ensure the stability and accuracy of lower diffusity and convection-dominated flows. In particular, we have employed second-order, unbounded, and conservative schemes for the diffusion terms, along with upwind schemes for the convection terms. These schemes are in-built in the OpenFoam library and are known for enhancing simulation stability by introducing artificial diffusion to adjust the Peclet number when necessary. The under-relaxation feature in the OpenFoam library was used to further stabilize the schemes and mitigate oscillations caused by smaller diffusion coefficients[106]. This under-relaxation technique, helps reduce oscillations and prevents the solution from blowing up. We specifically applied a relaxation factor of 0.3 across all equations.

The mesh was prepared to ensure the robustness and accuracy of the computation. The initial mesh consists of 14,601 hexahedra, with the region around the LAA being refined using the SnappyHexMesh utility[90] (Fig. 6, A). To test the accuracy of our computation, we conducted a robustness analysis

ACCEPTED MANUSCRIPT
Physics of Fluids
AIP Publishing
This is the author's peer reviewed, accepted manuscript. However, the online version of record will be different from this version once it has been copyedited and typeset.
PLEASE CITE THIS ARTICLE AS DOI: 10.1063/5.0216196

by comparing the results generated by the model when a normal mesh and a finer mesh are used (Fig. 6, B). The finer mesh consists of 66,891 hexahedral cells, which is 3.58 times denser than the standard mesh used. It was generated by increasing the resolution level in SnappyHexMesh utility. In the corresponding simulations, we computed the total concentration of fibrin mesh generated. Fig. 6, C shows the total amount of the generated fibrin polymer over time in simulations where the two meshes are employed. The relative error with respect to the used mesh at $t = 200\ s$ is 9.31%. The mesh consistency analysis for the chicken wing LAA case is provided in Appendix C. Table II summarizes the number of cells and the error obtained in each case.

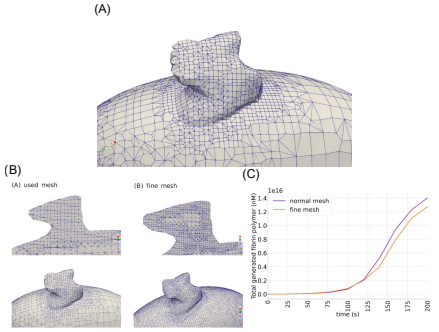

FIG. 6. (A) A snapshot of the computational mesh showing the refined areas which corresponds to the left atrium appendage and its surroundings. (B) The two numerical meshes used in the robustness analysis. (C) The total amount of the generated fibrin polymer over time in the simulations where the standard and finer mesh are used.

	chicken wing	cactus
Number of cells in the used mesh	13,937	14,601
Number of cells in the refined mesh	24,636	66.891
Error at $t = 200s$	1.84%	9.31%

TABLE II. A summary of the results of the mesh consistency study for both the chicken wing and cactus LA geometries.

III. RESULTS

A. Flow patterns in LAA during atrial fibrillation

We begin by investigating the patterns of flow velocity inside the LAA during a cardiac cycle in a patient with atrial fibrillation. We analyze the patterns of flow velocity streamlines at different moments of a pulsation cycle. Chicken wing LAA is characterized by a simple shape, smooth walls, a bending angle, and has an inlet diameter of 3.2 *cm*. Flow enters the LAA and leaves it depending on the phases of the pulsation cycle. As a result, it generates a vortex at the center of the LAA during the transition from the systolic to the diastolic phase (Fig. 7, A). Noteworthy is that the flow pattern near the LAA orifice in the modeled case of AF (when the walls are immobile) is different from the healthy cardiac cycle (when the LAA walls are contracting during the systole)[75]. Instead of the normal inflow/outflow streaming through the whole interior of the LAA, we observe the rotational motion of the fluid at the ostium with dominating tangential direction of the velocity field near the LAA entrance. This provides stasis conditions inside the LAA and favors thrombosis according to Virchow's triad. Strong and chaotic flow can also be observed at the entrance of the LAA. This generated vortex covers most of the LAA surface, except the tip. Indeed, the flow velocity is significantly lower at the tip of the chicken wing LAA as shown in the results presented in Appendix D, which provides favorable conditions for clotting initiation.

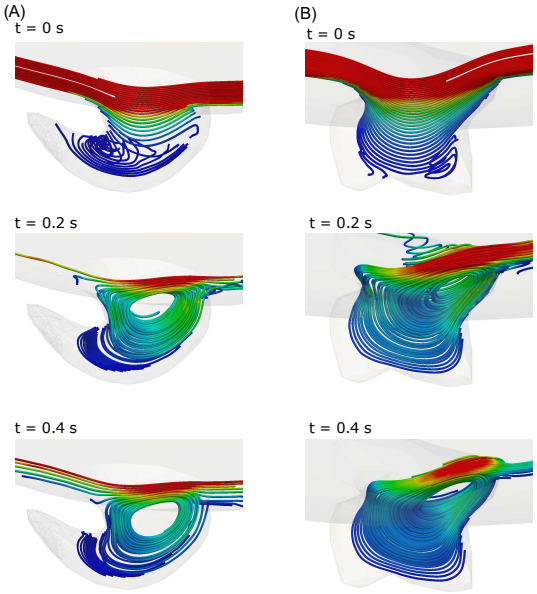

FIG. 7. Streamlines patterns showing flow dynamics inside the chicken wing (left) and cactus (right) LAA at different stages of the cardiac cycle. These simulations are conducted using the coagulation model and for validation purposes through comparison with the CFD model.

Next, we study clot development inside the LAA with a cactus shape. The cactus LAA is more irregular and complex and also has a larger inlet than its chicken wing counterpart (diameter of 3.34 *cm*). Flow dynamics are qualitatively similar to the chicken wing case. However, the relative vortex location is slightly closer to the entrance than the one observed in the chicken wing. Furthermore, flow circulation covers the entire surfaces of the LAA (Fig. 7, B). In order to study the effect of hydrodynamics on thrombus formation we further

AIP Publishing Physics of Fluids ACCEPTED MANUSCRIPT
This is the author's peer reviewed, accepted manuscript. However, the online version of record will be different from this version once it has been copyedited and typeset.
PLEASE CITE THIS ARTICLE AS DOI: 10.1063/5.0216196

consider two different cases corresponding to a reduced and an increased flow velocity, respectively.

B. Case I: reduced flow velocity

We consider a different inlet flow velocity such as the velocity magnitude at the entrance of the LAA is pulsating and reduced by approximately 10%, compared to the normal case. In these conditions, we evaluate the impact of the LAA shape on potential fibrin generation and clot formation. As by default conditions, we also assume that red blood cells occupy the whole LAA space at the beginning of our simulations and that the hematocrit value is equal to 0.3.

a. Effect of the LAA shape The shape of LAA influences clot formation in multiple ways. First, the influx of blood cells and zymogens involved in the coagulation process depends on the size of the LAA neck. Second, the internal flow patterns and wall shear stress vary according to the geometry of the LAA. In this context, the low wall shear stress and the access to procoagulant proteins and cells represent favorable conditions for the initiation of the coagulation process. This process starts when the tissue factor (TF) expressed on damaged walls is exposed to factors IX and X for a sufficiently long time. This is because an initial amount of thrombin needs to be generated for the amplification phase to start. The activation of these two proteins by the TF-FVIIa complex triggers the coagulation cascade, which culminates in the activation of prothrombin into thrombin. The latter does not only convert fibrinogen into fibrin, but also activates the platelets. Once activated, platelets promote coagulation in two ways. First, they accelerate the coagulation process by expressing procoagulant factors on their surface. Second, they form a porous medium that decelerates flow velocity and provides favorable conditions for fibrin polymerization.

Our simulations reproduce the dynamics of clot formation in both the chicken wing and cactus LAAs. In the chicken wing case, coagulation begins early in the simulation at the extremity of the tip (Fig. 8). This region is characterized by reduced wall shear stress. This suggests that the risk of clot formation at the tip is higher than near the entrance of the chicken wing LAA. A few seconds later, we start observing fibrin polymer in the neighborhood of the LAA entrance. By this time, the formed clot at the tip has already reached its final expansion. Our simulations suggest that the formation of the clot at the entrance of the LAA takes approximately 40 seconds after the moment of clot development at the tip. Indeed, clot formation starts around $t = 80\,s$ and continues until the end of the simulation. Note that the kinetics of the coagulation model were accelerated to reduce the computational time. Hence, the time points given here are the for the purpose of comparison and may not correspond to the actual time scales of LAA thrombosis. However, the extent to which the observed clot at the entrance propagates is also significantly higher. This is because the clot at the entrance is exposed to a continuous stream of inactive platelets and coagulation proteins, which sustains thrombin production.

The observed dynamics of clot formation in the cactus LAA

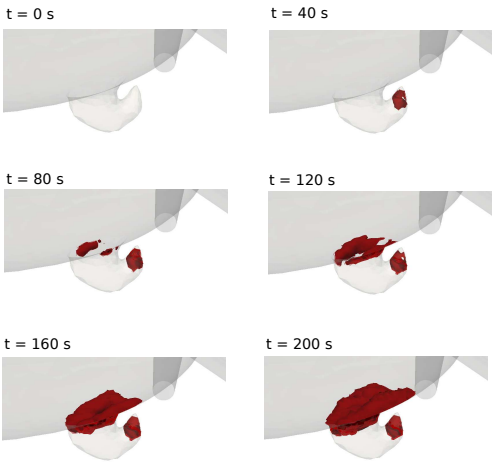

FIG. 8. Stages of clot formation in the chicken wing geometry. The red isovolumes correspond to portion of the computational domain where the fibrin polymer concentration exceeds 1000 *nM*.

are different than in the chicken wing one (Fig. 9). First, the generation of fibrin polymer is not observed until around $t = 80\,s$, suggesting that coagulation starts later than in the chicken wing case. At this time, while fibrin polymer is first generated in the vicinity of the LAA, it can also be slightly observed at the entrance of the LAA. These findings suggest that coagulation starts at the entrance and on the inner side of the LAA approximately at the same time. Another difference between the chicken wing and the cactus cases is that the development of the clot at the interior takes a longer time to complete in the cactus LAA. This is probably because the irregular and non-smooth edges of the cactus LAA contributes to the reduction of the wall shear stress, which promotes coagulation initiation. Further, the amount of generated fibrin polymer inside the LAA is significantly higher in the cactus case.

b. Effect of the initial blood composition in the LAA and the hematocrit on the risk of clot formation We took advantage of the fidelity of our modeling framework to elucidate the effects of the initial composition of the LAA on the risk of clot formation. We consider two scenarios corresponding to the situations where the LAA is initially occupied by either platelets or erythrocytes, and we calculate the total amount of generated fibrin polymer by the end of each simulation (Fig. 10, A). This is motivated by the uncertainty regarding the initial composition of LAA. In both scenarios, we observe that the formation of fibrin polymer in cactus is greater than in chicken wing LAAs. Further, coagulation is significantly enhanced when the LAA is initially filled with platelets. In other words, only platelets occupy the interior part of the LAA at the beginning of the simulations. In this context, our simulations suggest that platelets significantly increase fibrin poly-

ACCEPTED MANUSCRIPT
Physics of Fluids
AIP Publishing
This is the author's peer reviewed, accepted manuscript. However, the online version of record will be different from this version once it has been copyedited and typeset.
PLEASE CITE THIS ARTICLE AS DOI: 10.1063/5.0216196

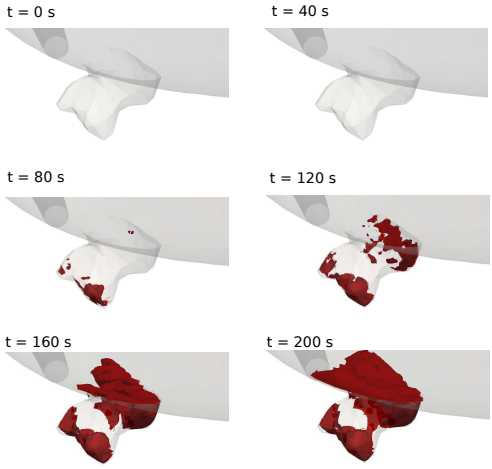

FIG. 9. Stages of clot formation in the cactus case. Red isovolumes represent the areas where the fibrin polymer concentration exceeds 1000 nM.

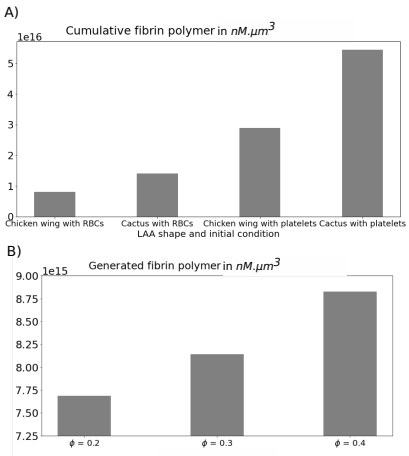

FIG. 10. The total amount of generated fibrin polymer by the end of the simulation for different LAA shapes and initial compositions (A), and for varying hematocrit values when the chicken wing case is considered (B).

mer production by 2.55- and 2.85-folds for the chicken wing and cactus morphologies, respectively

We continue our study by exploring the effect of the hematocrit on fibrin polymer production inside the LAA. Red blood cells influence coagulation directly, by activating resting platelets, and indirectly, through the margination of platelets and the upregulation of flow viscosity. We consider the case where a chicken wing LAA is initially filled with erythrocytes and simulate clot formation when three physiologically relevant values of the hematocrit are considered: 0.2, 0.3, and 0.5 (Fig. 10, B). Our simulations suggest that the hematocrit significantly influences the total amount of the generated fibrin polymer. Further, the hematocrit value correlates positively with the activity of coagulation. These findings suggest that high hematocrit could be an important risk factor for thrombogenesis in LAAs during atrial fibrillation. However, the effect of the hematocrit is less important in the case of thrombosis in cactus LAA as presented in Appendix E.

C. Case II: increased flow velocity

After studying the dynamics of clot formation in the case of reduced flow velocity, we consider the situation where flow circulation is increased. As we did previously, we begin by comparing the evolution of clot formation in chicken and cactus LAAs. Then, we study the effect of the initial cellular composition and the hematocrit level on fibrin polymer generation. To allow coagulation initiation, we increase the expression of tissue factor on damaged areas by 10 times. This is because higher flow velocity prevents coagulation initiation if the same concentration of TF is maintained. Further, we consider that LAA is initially composed of erythrocytes and that the hematocrit level is 0.3, as the default conditions in our simulations.

a. Effect of the LAA shape Increased flow velocity has different effects on the coagulation process in the LAA. On one hand, it prevents the inactive coagulation proteins and cells from staying for a sufficient duration in proximity to the damaged tissues. Hence, it reduces the chances of clot initiation. Further, it removes active coagulation proteins and platelets and limits the generation of thrombin. On the other hand, increased flow circulation upregulates the influx of inactive coagulation proteins and cells into the LAA. Increased flow velocity also promotes the margination of platelets by red blood cells.

We provide numerical simulations where we compare the development of the clot in LAAs with chicken wing and cactus shapes (Fig. 11). In the case of chicken wing, fibrin polymer generation becomes noticeable after around 150 s of the simulation start. However, contrary to the situation where the flow velocity is decreased, coagulation starts at both the tip and the entrance approximately at the same time. Further, the development of the clot at the entrance occurs faster when flow velocity increases. This is probably because the faster flow transports more platelets and procoagulant factors to this area. The same dynamics of clot growth can be observed in the cactus LAA. However, the produced fibrin polymer becomes noticeable significantly earlier at both the inner side and the entrance of the LAA domain. It reaches a steady state after approximately 120 s of the simulation start. These dynamics suggest that increased flow velocity promotes the development of simultaneous clot formation in different regions

ACCEPTED MANUSCRIPT
Physics of Fluids
AIP Publishing
This is the author's peer reviewed, accepted manuscript. However, the online version of record will be different from this version once it has been copyedited and typeset.
PLEASE CITE THIS ARTICLE AS DOI: 10.1063/5.0216196

of the LAA.

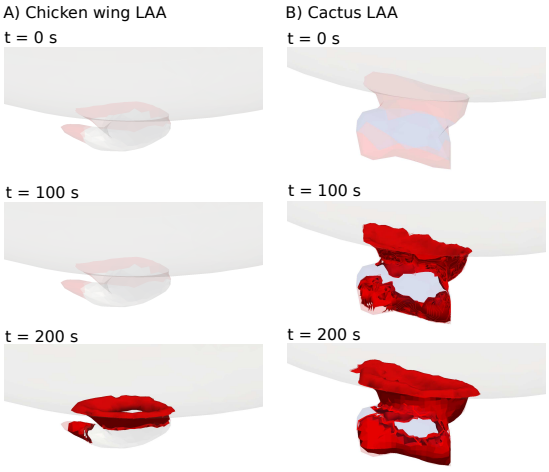

FIG. 11. Stages of clot growth inside a chicken wing and cactus LAAs in the case of increased flow velocity. Red isovolumes correspond to regions where fibrin polymer concentration exceeds 1000 *nM*.

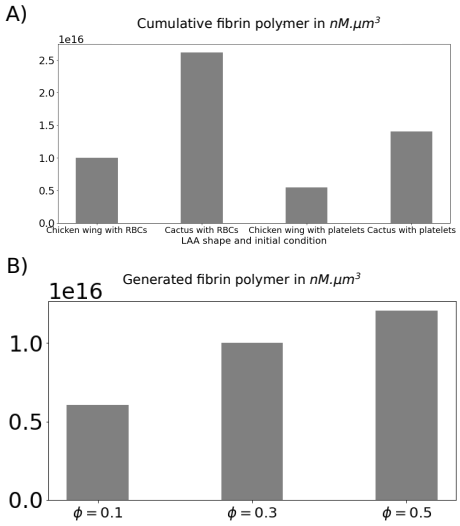

FIG. 12. The cumulative amount of generated fibrin polymer when considering different initial conditions corresponding to cases where platelets or RBCs occupy the LAA (A) and for different hematocrit levels (B).

b. Contribution of the initial composition of the LAA and the hematocrit We took advantage of the multiphase approach to study the contribution of platelets and erythrocytes to thrombogenesis in LAA. We begin by investigating the impact of the cell composition inside the LAA at the beginning of the coagulation process. We consider two different initial conditions corresponding to the cases where platelets or RBCs occupy the LAA. Then, we compute the amount of fibrin polymer generated by the end of the simulation. Contrary to the case where the blood flow velocity is low, fibrin polymer generation increases when the LAA is initially filled with red blood cells.

We evaluate the effect of the hematocrit on the development of the clot in the LAA. We consider the situation where a chicken wing LAA is initially filled with red blood cells, and consider three physiological hematocrit levels: low (10%), normal (30%), and high (50%) (Fig. 12, B). In this case, reducing the hematocrit level from 30% to 10% decreases the generated fibrin polymer by 39.57%, while increasing it from 30% to 50% upregulates the cumulative generation of fibrin polymer by 20.68%. These findings suggest an important role of red blood cells in the case where flow circulation is fast.

IV. DISCUSSION

Thrombosis in the left atrial appendage (LAA) is a life threatening pathology, often associated with atrial fibrillation (AF). The irregular and often fast heart rate in AF can cause insufficient blood flow in the LAA, creating a predisposition for clot formation. AF can lead to changes in the atrial tissue, further promoting thrombus formation. Stroke is the primary concern of LAA thrombus formation, as thrombi can embolize to the cerebral arteries, leading to ischemic stroke. Thrombi can also travel to other parts of the body, causing infarctions in organs like the kidneys or intestines. Treatment includes anticoagulation therapy with warfarin or direct oral anticoagulants, restoring normal heart rhythm electrically or pharmacologically, catheter ablation or LAA occlusion.

A. LAA thrombosis modelling

The importance of mathematical modeling of thrombosis in the LAA is multifaceted, encompassing enhanced understanding of underlying mechanisms, improved risk prediction and patient-specific care, optimization of therapeutic interventions, advancement of research, and better healthcare resource management. These models serve as powerful tools in the quest to mitigate the risks and consequences of thromboembolic events, ultimately contributing to better patient outcomes and more efficient healthcare delivery.

The complexity of LAA thrombosis modelling arises from the need to accurately represent the intricate and patient-specific anatomical structures, complex and highly variable blood flow, the detailed biochemical interactions, and the integration of processes occurring at multiple scales and time frames.

AIP Publishing Physics of Fluids ACCEPTED MANUSCRIPT
This is the author's peer reviewed, accepted manuscript. However, the online version of record will be different from this version once it has been copyedited and typeset.
PLEASE CITE THIS ARTICLE AS DOI: 10.1063/5.0216196

In this study, we introduced a new framework for patient-specific LAA thrombosis prediction, integrating data from computed tomography, electrocardiography, and dopplerography. This innovative approach pioneers the application of multiphase models for coagulation, combining platelet aggregation, precise biorheology, and blood plasma biochemistry in LAA thrombosis modeling. As a result, it allowed us to investigate complex biomedical questions, such as the contribution of hematocrit and the initial concentration of blood cells in the LAA. The complexity of blood flow in the left atrium is driven by its complex patient-specific anatomy, the dynamic nature of cardiac cycles, interaction with the mitral valve, variability of pulmonary venous inflows, and patient-specific factors. Advanced computational techniques and high-resolution modeling are essential to accurately simulate and understand these complex flow patterns, ultimately contributing to better diagnostic and therapeutic strategies for conditions like atrial fibrillation and thrombus formation.

We started by studying the patterns of blood flow inside two patient-specific left atrium geometries. To achieve this, we used a computational fluid dynamics model and parameterized it to the measured flow velocities at various parts of the left atrium in patients with atrial fibrillation (AF). Our simulations suggest the development of vortices at the entrance of LAAs, which sometimes extend to the inner part, depending on the phases of the atrial fibrillation pulsations. Due to the uncertainties regarding the values of flow velocity at the entrance of the LAA, we considered two cases corresponding to two values of inlet flow velocities.

B. The role of LAA geometry, platelets, hematocrit

We took advantage of the flexibility and fidelity of our multiphase model to identify the main factors contributing to the formation of thrombosis inside LAAs. We run several numerical simulations corresponding to various scenarios which reflect physiological situations with different shapes of the LAA, initial cell compositions, and hematocrit levels.

Across all scenarios, the generation of fibrin polymer is significantly increased in the cactus LAAs. This is probably due to a combination of factors including the larger inlet radius and the complex shape of cactus LAAs relative to chicken wing ones. Further, our simulations suggest that reduced flow velocity promotes the development of the clot inside the LAA, while faster flow circulation results in the initiation of coagulation at the both inside and the entrance of the LAA. According to clinical reports, "the larger LAA orifice and non-chicken wing shape LAA are independent factors of decreased mechanical function of LAA"[107], hence these conditions can be characterized by increased ricks of thrombosis. Another recent study reports that "large LAA orifice area (...) and slow internal velocity (...) were found to be significant risk factors of stroke"[108]. Our simulations are qualitatively coherent with these observations.

Another difference in the observed dynamics concerns the contribution of platelets and red blood cells. Our findings show that the initial prevalence of platelets inside the LAA upregulates the generation of fibrin polymer when flow velocity is low. However, it is the prevalence of erythrocytes that promotes coagulation when flow circulation is faster. This is probably because high flow velocity prevents the platelets from aggregating near the injured areas. Finally, our model suggests that increased hematocrit levels can significantly promote the generation of fibrin polymer. It was previously shown that increased hematocrit is a risk factor for venous thrombosis[10,109]. A previous modeling study has suggested the importance of considering hematocrit-dependent rheology to properly simulate blood stasis in LAA[110]. Indeed, It was shown that considering non-Newtonian flow rheology changes the size of vortices and stagnation areas inside the LAA[111]. Another study underscored the importance of LAA shape in the process of clot formation[112].

C. Limitations and further perspectives

Overall, our study provides some key qualitative insights into the complex process of thrombosis inside LAA. These insights can help us to improve our understanding of this process and identify therapeutic targets which can lead to the development of new treatments. It is important to note that our study has several limitations. First, the velocity at the entrance of the LAA was modeled by a computational fluid dynamics (CFD) code assuming patient-specific geometries, however, the clot growth modeling was implemented under the assumption of idealized geometry. The differences in the geometries of the left atrium portion used in the CFD simulations and the one considered in the clotting simulation can lead to small discrepancies in the simulated flow velocity field. Further, we restricted this study to rigid geometries because taking into account the tissue deformation would make the simulations computationally prohibitive and requires extensive validation using fluid-structure interaction benchmarks.

The immobile LAA walls are characteristic of atrial fibrillation that we aim to simulate, as opposed to the normal sinus rhythm. This fact changes the flow pattern at the LAA orifice, as shown in Ref.[75]. In that sense, the solid-wall assumption for the LAA model no longer seems to be a limitation, but rather a physiological condition. Of course, there is some wall elasticity that we miss in the present model, and in fact, during AF there are small wall oscillations (which create some additional blood motion near the endocardium), but these deformations are negligible compared to the active contraction. As for the atrium walls, indeed, the solid-wall assumption reduces the computational costs. Instead, we use the simplified geometry for the atrium and tune the boundary conditions to mimic the fluid dynamics in the vicinity of the LAA neck. Besides, since there is no exact data on the displacement of the atrial wall in time, it is logical to omit the unnecessary complication. However, the combination of the FSI with the multiphase thrombosis modeling seems achievable in near future. Taking into consideration of the wall motion may potentially increase the clot formation time because of arising near-wall fluid velocity that may disrupt the fibrin polymerization. Nonetheless, the presented results provide a compar-

ACCEPTED MANUSCRIPT
Physics of Fluids
AIP Publishing
This is the author's peer reviewed, accepted manuscript. However, the online version of record will be different from this version once it has been copyedited and typeset.
PLEASE CITE THIS ARTICLE AS DOI: 10.1063/5.0216196

ative numerical analysis of the clot formation process in LAA for two patient-specific geometries and for the two scenarios regarding the fluid velocity magnitude at the entrance of the LAA.

Another point of further modification of the proposed model could be the implementation of a shear-induced mechanism for platelet aggregation, which is attributed to conformational changes in von Willebrand factor (VWF) protein caused by hydrodynamic forces[113–115]. This effect is relevant at high shear rates in the blood ($> 5000\ s^{-1}$)[116], and in the considered case of stagnant low-shear LAA flows typical for AF[74] such shear-triggered platelet aggregation should be inhibited (at least for the healthy VWF). Noteworthy, several clinical studies indicate that VWF expression by the atrial endocardium may be a prognostic factor for thrombotic events and AF outcomes[117–120], yet current findings are controversial and require additional investigation. Additionally, our current model implementation assumes that the clot displays the same hydraulic resistance against both the plasma and RBCs phases. In *in vivo* conditions, erythrocytes cannot penetrate the clot due to the small size of its pores.

It also should be mentioned that we are not considering mobile thrombi in the present paper. In this model, we investigate the initiation of thrombosis by the expression of TF on LAA wall patches. Hence, we focus on the *mural* thrombi, described in medical literature[25,91,121]. Those are related and usually triggered by wall damage or inflammation in the endocardial endothelium. Such mural thrombi may indeed become mobile due to adverse hemodynamic conditions and the resulting high forces exerted on them. This could be modeled with the proposed framework in principle, but it escapes from the scope of the present study.

V. CONCLUSION

In the present work, we developed a novel multi-scale and multi-physics approach to the patient-specific numerical analysis of thrombosis dynamics in the LAA during atrial fibrillation. We combined various techniques of computerized X-ray tomography imaging, digitization, and computational fluid dynamics with a validated multiphase continuum thrombosis model that accounts for the time-dependent blood flows, the non-Newtonian rheology, the biochemical cascade of clotting reactions, the two-stage platelet aggregation and activation together with the multifaceted role of erythrocytes. Recently, there have been an interest in developing such methods for LAA diagnosis and treatment. Further, some of the proposed methods include 3D printing, in addition to CT-scans and CFD[122–124], while others have considered AI-enabled computational simulations to facilitate the decision-making of surgeons performing LAA closure[125]. Our study shows the advantage of using a multiphase model of coagulation which encompasses the main features influencing clot formation in LAAs, including the rheological, cellular, and molecular aspects. Our simulations suggest that LAA thrombosis is sensitive to hematocrit, geometry and orifice size. Hopefully, the findings of the present paper could help in the identification of novel anti-thrombotic therapies and in early diagnostics of adverse cardiovascular events in patients with atrial fibrillation.

APPENDIX A: LIST OF MODEL SPECIES

A summary of of the variables used in the present work is provided in Table III.

Variable	Description	Units
P_f	concentration of platelets in flow	$\times 10^{-9}\ L$
P_c^1	concentration of aggregated platelets	$\times 10^{-9}\ L$
P_c^2	concentration of strongly activated platelets	$\times 10^{-9}\ L$
U	concentration of activated factor X	nM
P	concentration of prothrombin	nM
T	concentration of thrombin	nM
A	concentration of antithrombin	nM
F_g	concentration of fibrinogen	nM
F	concentration of fibrin	nM
F_p	concentration of polymerized fibrin	nM
$\mathbf{v}$	two-phase fluid velocity	m/s
$\mathbf{v}_p$	blood plasma velocity	m/s
$\mathbf{v}_s$	velocity of RBC phase	m/s
p	fluid pressure	Pa
ϕ	RBC-phase fraction	non-dimensional

TABLE III. A summary of all variables used in the model.

APPENDIX B: EXPERIMENTAL VALIDATION OF THE MULTIPHASE MODEL

In this section, we briefly recall the validation the model against experiments reported in Refs.[126,127], where MRI tracked thrombus shape evolution over 90 minutes. The blood samples had a hematocrit of around 30%. The thrombus reached its maximal expansion in about 30 minutes[127]. The final clot shape and size in our simulations matched experimental observations, but clot growth was accelerated to optimize computational time.

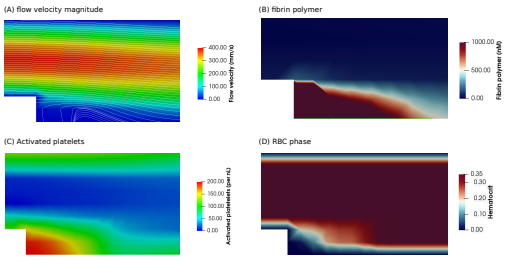

FIG. 13. The final stage of clot formation in backward-facing step geometry with conditions replicating those of experiments[126]. (A) The velocity magnitude profile, (B) The fibrin polymer concentration, (C) The active platelets density, and (D) the RBC phase fraction.

ACCEPTED MANUSCRIPT
Physics of Fluids
AIP Publishing
This is the author's peer reviewed, accepted manuscript. However, the online version of record will be different from this version once it has been copyedited and typeset.
PLEASE CITE THIS ARTICLE AS DOI: 10.1063/5.0216196

We examined clot growth in a recirculation area created in a backward-facing step (BFS) domain[52,126]. The BFS domain was placed in a fluid loop with a peristaltic pump driving the blood flow. The BFS had a 10 mm diameter, and the step height was 2.5 mm. The inlet flow rate was adjusted to achieve an inlet velocity of 0.2 m/s. We used a 2D geometry for the BFS model and generated a numerical mesh with 4258 hexahedral cells. Fig. 13 shows the obtained steady-state field value for the flow velocity, the fibrin polymer, the activated platelets, and the RBC phase. Similarily to the experiments, the model showed a strong dependency of thrombus length on hematocrit[52]. It predicts that at steady state, the thrombus will have a length of 10 *mm* and a height of 2.27 *mm*. In the experiments[126], the thrombus had a length and height of 9.7 *mm* and 2.3 *mm*, respectively. RBCs appear to push platelets into the corner, limiting thrombus growth. We defined thrombus regions by fibrin polymer concentrations higher than 350 nM. To reduce computational costs, we tuned parameters so the thrombus reaches its stable size in about 250 seconds.

APPENDIX C: CONSISTENCY ANALYSIS FOR THE CHICKEN WING MESH

In this section, we present the results of the mesh consistency evaluation for the chicken wing LAA case. We refined the mesh using the SnappyHexMesh utility and repeated the simulation to calculate fibrin polymer production over time. The original mesh contains 13,937 hexahedral cells, while the refined mesh consists of 24,636 cells. Fig. 14 displays both meshes and the corresponding simulation results.

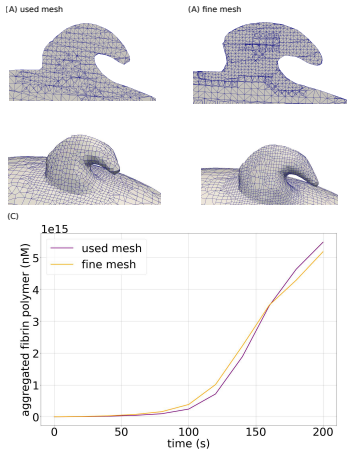

FIG. 14. Two screenshots showing the used mesh in the simulations (A) and the refined mesh considered in the consistency analysis (B). The simulation results obtained using each of the two meshes are displayed (C).

APPENDIX D: FLOW VELOCITY MAGNITUDE INSIDE THE LAA

The magnitude of flow velocity in the chicken wing and cactus LAAs is provided in Fig. 15.

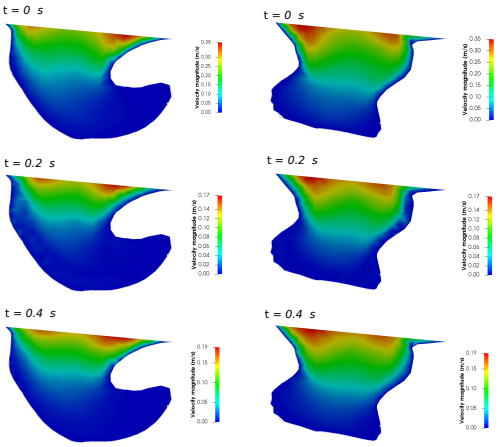

FIG. 15. The magnitude of flow velocity across a section of the chicken wing (left) and cactus (right) LAAs during different moment of a pulsation cycle.

APPENDIX E: A COMPARISON BETWEEN THE EFFECT OF THE HEMATOCRIT IN CHICKEN WING AND CACTUS GEOMETRIES

In this section, we evaluate the effect of hematocrit on fibrin polymer production. Fig. 16 shows the concentration of fibrin polymer generated in chicken wing and cactus geometries for different hematocrit values in the reduced flow case.

ACKNOWLEDGEMENTS

G.P. and N.K. are supported by European Social Fund (project No 09.3.3-LMT-K-712-17-003) under a grant agreement with the Research Council of Lithuania (LMTLT). A.V.B. acknowledges the support from the State Scientific Program of Russian Federation (Faculty of Physics, Moscow State University, no.122091200035-7). We are grateful to Prof. S.Borodinas for useful discussions, to Dr. O.Ardatov for the Solidworks implementation of computed tomography imaging. V.V. has been supported by the RUDN University Strategic Academic Leadership Program.

ACCEPTED MANUSCRIPT
Physics of Fluids
AIP Publishing
This is the author's peer reviewed, accepted manuscript. However, the online version of record will be different from this version once it has been copyedited and typeset.
PLEASE CITE THIS ARTICLE AS DOI: 10.1063/5.0216196

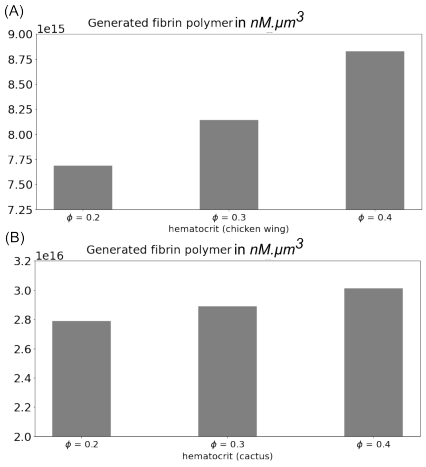

FIG. 16. The magnitude of flow velocity across a section of the chicken wing (left) and cactus (right) LAAs during different moment of a pulsation cycle.

DECLARATIONS

- **Competing interests**: We declare no conflict of interests.
- **Funding**: G.P. and N.K. are supported by European Social Fund (project No 09.3.3-LMT-K-712-17-003) under a grant agreement with the Research Council of Lithuania (LMTLT). A.V.B. acknowledges the support from the State Scientific Program of Russian Federation (Faculty of Physics, Moscow State University, no.122091200035-7). The sources of funding provided merely a financial support and had no involvement in the study design, nor in the collection, analysis and interpretation of data, nor in the writing of the manuscript, nor in the decision to submit the manuscript for publication.
- **Availability of data and materials**: Raw data and materials may be obtained from the corresponding author upon a reasonable request.

[1]F. C. Roessler, N. Kalms, F. Jann, A. Kemmling, J. Ribbat-Idel, F. Stellmacher, I. R. König, M. Ohlrich, and G. Royl, "First approach to distinguish between cardiac and arteriosclerotic emboli of individual stroke patients applying the histological THROMBEX-classification rule," Scientific Reports **11** (2021), 10.1038/s41598-021-87584-2.
[2]T. Boeckh-Behrens, J. F. Kleine, C. Zimmer, F. Neff, F. Scheipl, J. Pelisek, L. Schirmer, K. Nguyen, D. Karatas, and H. Poppert, "Thrombus histology suggests cardioembolic cause in cryptogenic stroke," Stroke **47**, 1864–1871 (2016).
[3]J. Romero, J. J. Cao, M. J. Garcia, and C. C. Taub, "Cardiac imaging for assessment of left atrial appendage stasis and thrombosis," Nature Reviews Cardiology **11**, 470–480 (2014).
[4]N. M. Al-Saady, O. A. Obel, and A. J. Camm, "Left atrial appendage: structure, function, and role in thromboembolism," Heart **82**, 547–554 (1999).
[5]A. Cresti, M. A. García-Fernández, H. Sievert, P. Mazzone, P. Baratta, M. Solari, A. Geyer, F. De Sensi, and U. Limbruno, "Prevalence of extra-appendage thrombosis in non-valvular atrial fibrillation and atrial flutter in patients undergoing cardioversion: a large transoesophageal echo study," EuroIntervention **15**, e225–e230 (2019).
[6]M. Roy, A. K. Roy, J. R. DeSanto, and M. Abdelsalam, "Free floating thrombus in carotid artery in a patient with recurrent strokes," Case Reports in Medicine **2017**, 1–4 (2017).
[7]O. D. Backer, S. Arnous, N. Ihlemann, N. Vejlstrup, E. Jørgensen, S. Pehrson, T. D. W. Krieger, P. Meier, L. Søndergaard, and O. W. Franzen, "Percutaneous left atrial appendage occlusion for stroke prevention in atrial fibrillation: an update," Open Heart **1**, e000020 (2014).
[8]F. K. Wegner, R. Radke, C. Ellermann, J. Wolfes, A. J. Fischer, H. Baumgartner, L. Eckardt, G.-P. Diller, and S. Orwat, "Incidence and predictors of left atrial appendage thrombus on transesophageal echocardiography before elective cardioversion," Scientific Reports **12** (2022), 10.1038/s41598-022-07428-5.
[9]M. Markl, D. C. Lee, N. Furiasse, M. Carr, C. Foucar, J. Ng, J. Carr, and J. J. Goldberger, "Left atrial and left atrial appendage 4d blood flow dynamics in atrial fibrillation," Circulation: Cardiovascular Imaging **9** (2016), 10.1161/circimaging.116.004984.
[10]A. Gonzalo, M. García-Villalba, L. Rossini, E. Durán, D. Vigneault, P. Martínez-Legazpi, O. Flores, J. Bermejo, E. McVeigh, A. M. Kahn, *et al.*, "Non-newtonian blood rheology impacts left atrial stasis in patient-specific simulations," International Journal for Numerical Methods in Biomedical Engineering **38**, e3597 (2022).
[11]A. Qureshi, M. Balmus, D. Nechipurenko, F. Ataullakhanov, S. Williams, G. Lip, D. Nordsletten, O. Aslanidi, and A. de Vecchi, "Left atrial appendage morphology impacts thrombus formation risks in multi-physics atrial models," in *2021 Computing in Cardiology (CinC)* (IEEE, 2021).
[12]A. Qureshi, G. Y. Lip, D. A. Nordsletten, S. E. Williams, O. Aslanidi, and A. De Vecchi, "Imaging and biophysical modelling of thrombogenic mechanisms in atrial fibrillation and stroke," Frontiers in Cardiovascular Medicine **9**, 1074562 (2023).
[13]G. M. Bosi, A. Cook, R. Rai, L. J. Menezes, S. Schievano, R. Torii, and G. Burriesci, "Computational fluid dynamic analysis of the left atrial appendage to predict thrombosis risk," Frontiers in Cardiovascular Medicine **5** (2018), 10.3389/fcvm.2018.00034.
[14]X. Morales, J. Mill, K. A. Juhl, A. Olivares, G. Jimenez-Perez, R. R. Paulsen, and O. Camara, "Deep learning surrogate of computational fluid dynamics for thrombus formation risk in the left atrial appendage," in *Statistical Atlases and Computational Models of the Heart. Multi-Sequence CMR Segmentation, CRT-EPiggy and LV Full Quantification Challenges* (Springer International Publishing, 2020) pp. 157–166.
[15]G. Y. Lip, "Intracardiac thrombus formation in cardiac impairment: the role of anticoagulant therapy." Postgraduate Medical Journal **72**, 731–738 (1996).
[16]A. Fleddermann, R. Eckert, P. Muskala, C. Hayes, A. Magalski, and M. L. Main, "Efficacy of direct acting oral anticoagulant drugs in treatment of left atrial appendage thrombus in patients with atrial fibrillation," The American Journal of Cardiology **123**, 57–62 (2019).
[17]E. Caliskan, J. L. Cox, D. R. Holmes, B. Meier, D. R. Lakkireddy, V. Falk, S. P. Salzberg, and M. Y. Emmert, "Interventional and surgical occlusion of the left atrial appendage," Nature Reviews Cardiology **14**, 727–743 (2017).
[18]P. Cepas-Guillén, E. Flores-Umanzor, N. Leduc, V. Bajoras, N. Perrin, J. Farjat-Pasos, A. McInerney, A. Lafond, X. Millán, S. Zendjebil, *et al.*, "Impact of device implant depth after left atrial appendage occlusion," Cardiovascular Interventions **16**, 2139–2149 (2023).
[19]A. Akinapelli, O. Bansal, J. P. Chen, A. Pflugfelder, N. Gordon, K. Stein, B. Huibregtse, and D. Hou, "Left atrial appendage closure –the WATCHMAN device," Current Cardiology Reviews **11**, 334–340 (2015).
[20]D. N. Majule, C. Jing, W. M. Rutahoile, and F. S. Shonyela, "The efficacy and safety of the WATCHMAN device in LAA occlusion in patients with non-valvular atrial fibrillation contraindicated to oral anticoagulation: A focused review," Annals of Thoracic and Cardiovascular Surgery **24**, 271–278 (2018).

AIP Publishing Physics of Fluids ACCEPTED MANUSCRIPT
This is the author's peer reviewed, accepted manuscript. However, the online version of record will be different from this version once it has been copyedited and typeset.
PLEASE CITE THIS ARTICLE AS DOI: 10.1063/5.0216196

[21]A. Sedaghat, V. Vij, B. Al-Kassou, S. Gloekler, R. Galea, M. Fürholz, B. Meier, M. Valgimigli, G. O'Hara, D. Arzamendi, V. Agudelo, L. Asmarats, X. Freixa, E. Flores-Umanzor, O. D. Backer, L. Søndergaard, L. Nombela-Franco, A. McInerney, K. Korsholm, J. E. Nielsen-Kudsk, S. Afzal, T. Zeus, F. Operhalski, B. Schmidt, G. Montalescot, P. Guedeney, X. Iriart, N. Miton, J. Saw, T. Gilhofer, L. Fauchier, E. Veliqi, F. Meincke, N. Petri, P. Nordbeck, S. Rycerz, D. Ognerubov, E. Merkulov, I. Cruz-González, R. Gonzalez-Ferreiro, D. L. Bhatt, A. Laricchia, A. Mangieri, H. Omran, J. W. Schrickel, J. Rodes-Cabau, and G. Nickenig, "Device-related thrombus after left atrial appendage closure: Data on thrombus characteristics, treatment strategies, and clinical outcomes from the EUROC-DRT-registry," Circulation: Cardiovascular Interventions **14** (2021), 10.1161/circinterventions.120.010195.

[22]P. B. Bertrand, M. Habran, K. Kenis, J. Lecomte, L. Moonen, D. Stroobants, and E. Benit, "Dual antiplatelet therapy after percutaneous left atrial appendage occlusion: single center experience with the amplatzer cardiac plug," Acta Cardiologica **74**, 74–81 (2018).

[23]J. Saw, J. E. Nielsen-Kudsk, M. Bergmann, M. J. Daniels, A. Tzikas, M. Reisman, and B. S. Rana, "Antithrombotic therapy and device-related thrombosis following endovascular left atrial appendage closure," JACC: Cardiovascular Interventions **12**, 1067–1076 (2019).

[24]X. Iriart, G. Blanc, X. P. Bouteiller, B. Legghe, B. Bouyer, S. Sridi-Cheniti, A. Bustin, C. Vasile, J.-B. Thambo, M. Elbaz, *et al.*, "Clinical implications of ct-detected hypoattenuation thickening on left atrial appendage occlusion devices," Radiology **308**, e230462 (2023).

[25]T. Saito, K. Tamura, D. Uchida, T. Saito, T. Nitta, and Y. Sugisaki, "Histopathological evaluation of left atrial appendage thrombogenesis removed during surgery for atrial fibrillation," American Heart Journal **153**, 704–711 (2007).

[26]K. Dudzińska-Szczerba, P. Kułakowski, I. Michałowska, and J. Baran, "Association between left atrial appendage morphology and function and the risk of ischaemic stroke in patients with atrial fibrillation," Arrhythmia & Electrophysiology Review **11** (2022), 10.15420/aer.2022.08.

[27]B. Kreidieh and M. Valderrábano, "Malignant left atrial appendage morphology and embolization risk in atrial fibrillation," HeartRhythm Case Reports **1**, 406–410 (2015).

[28]A. Masci, L. Barone, L. Dedè, M. Fedele, C. Tomasi, A. Quarteroni, and C. Corsi, "The impact of left atrium appendage morphology on stroke risk assessment in atrial fibrillation: A computational fluid dynamics study," Frontiers in Physiology **9** (2019), 10.3389/fphys.2018.01938.

[29]R. M. Heppell, K. E. Berkin, J. M. McLenachan, and J. A. Davies, "Haemostatic and haemodynamic abnormalities associated with left atrial thrombosis in non-rheumatic atrial fibrillation." Heart **77**, 407–411 (1997).

[30]R. J. Zotz, M. Müller, S. Genth-Zotz, and H. Darius, "Spontaneous echo contrast caused by platelet and leukocyte aggregates?" Stroke **32**, 1127–1133 (2001).

[31]T. Ito and M. Suwa, "Left atrial spontaneous echo contrast: relationship with clinical and echocardiographic parameters," Echo Research & Practice **6**, R65–R73 (2019).

[32]B. Wang, Z. Wang, G. Fu, B. He, H. Wang, W. Zhuo, S. Zhang, and H. Chu, "Left atrial spontaneous echo contrast and ischemic stroke in patients undergoing percutaneous left atrial appendage closure," Frontiers in Cardiovascular Medicine **8** (2021), 10.3389/fcvm.2021.723280.

[33]Y. Zhao, L. Ji, J. Liu, J. Wu, Y. Wang, S. Shen, S. Guo, R. Jian, G. Chen, X. Wei, W. Liao, S. Kutty, Y. Liao, and J. Bin, "Intensity of left atrial spontaneous echo contrast as a correlate for stroke risk stratification in patients with nonvalvular atrial fibrillation," Scientific Reports **6** (2016), 10.1038/srep27650.

[34]G. S. Reeder, J. E. Charlesworth, and S. B. Moore, "Cause of spontaneous echocardiographic contrast as assessed by scanning electron microscopy," Journal of the American Society of Echocardiography **7**, 169–173 (1994).

[35]T. Watson, E. Shantsila, and G. Y. Lip, "Mechanisms of thrombogenesis in atrial fibrillation: Virchow's triad revisited," The Lancet **373**, 155–166 (2009).

[36]C. E. Hansen, Y. Qiu, O. J. McCarty, and W. A. Lam, "Platelet mechanotransduction," Annual Review of Biomedical Engineering **20**, 253–275 (2018).

[37]T. J. Stalker, E. A. Traxler, J. Wu, K. M. Wannemacher, S. L. Cermignano, R. Voronov, S. L. Diamond, and L. F. Brass, "Hierarchical organization in the hemostatic response and its relationship to the platelet-signaling network," Blood **121**, 1875–1885 (2013).

[38]B. Furie and B. C. Furie, "Thrombus formation in vivo," J. Clin. Invest. **115**, 3355–3362 (2005).

[39]M. A. Panteleev, A. N. Balandina, E. N. Lipets, M. V. Ovanesov, and F. I. Ataullakhanov, "Task-oriented modular decomposition of biological networks: Trigger mechanism in blood coagulation," Biophysical Journal **98**, 1751–1761 (2010).

[40]N. A. Podoplelova, A. N. Sveshnikova, Y. N. Kotova, A. Eckly, N. Receveur, D. Y. Nechipurenko, S. I. Obydennyi, I. I. Kireev, C. Gachet, F. I. Ataullakhanov, P. H. Mangin, and M. A. Panteleev, "Coagulation factors bound to procoagulant platelets concentrate in cap structures to promote clotting," Blood **128**, 1745–1755 (2016).

[41]F. Swieringa, H. M. Spronk, J. W. Heemskerk, and P. E. van der Meijden, "Integrating platelet and coagulation activation in fibrin clot formation," Research and Practice in Thrombosis and Haemostasis **2**, 450–460 (2018), https://onlinelibrary.wiley.com/doi/pdf/10.1002/rth2.12107.

[42]K. Leiderman and A. L. Fogelson, "Grow with the flow: a spatial–temporal model of platelet deposition and blood coagulation under flow," Mathematical medicine and biology: a journal of the IMA **28**, 47–84 (2011).

[43]A. L. Fogelson and K. B. Neeves, "Fluid mechanics of blood clot formation," Annual Review of Fluid Mechanics **47**, 377–403 (2015).

[44]A. M. Shibeko, E. S. Lobanova, M. A. Panteleev, and F. I. Ataullakhanov, "Blood flow controls coagulation onset via the positive feedback of factor VII activation by factor Xa," BMC Systems Biology **4**, 5 (2010).

[45]A. Bouchnita, T. Galochkina, P. Kurbatova, P. Nony, and V. Volpert, "Conditions of microvessel occlusion for blood coagulation in flow," International journal for numerical methods in biomedical engineering **33**, e2850 (2017).

[46]A. V. Belyaev, M. A. Panteleev, and F. I. Ataullakhanov, "Threshold of microvascular occlusion: Injury size defines the thrombosis scenario," Biophysical Journal **109**, 450–456 (2015).

[47]S. P. Jackson, W. S. Nesbitt, and E. Westein, "Dynamics of platelet thrombus formation," Journal of Thrombosis and Haemostasis **7**, 17–20 (2009).

[48]S. P. Jackson, "Arterial thrombosis—insidious, unpredictable and deadly," Nature Medicine **17**, 1423–1436 (2011).

[49]L. F. Brass and S. L. Diamond, "Transport physics and biorheology in the setting of hemostasis and thrombosis," Journal of Thrombosis and Haemostasis **14**, 906–917 (2016).

[50]J. Stone, P. Hangge, H. Albadawi, A. Wallace, F. Shamoun, M. G. Knuttien, S. Naidu, and R. Oklu, "Deep vein thrombosis: pathogenesis, diagnosis, and medical management," Cardiovascular Diagnosis and Therapy **7** (2017).

[51]M. Lehmann, R. M. Schoeman, P. J. Krohl, A. M. Wallbank, J. R. Samaniuk, M. Jandrot-Perrus, and K. B. Neeves, "Platelets drive thrombus propagation in a hematocrit and glycoprotein vi–dependent manner in an in vitro venous thrombosis model," Arterioscler Thromb Vasc Biol **38**, 1052–1062 (2018).

[52]A. Bouchnita, A. V. Belyaev, and V. Volpert, "Multiphase continuum modeling of thrombosis in aneurysms and recirculation zones," Physics of Fluids **33**, 093314 (2021).

[53]M. O. Bernabeu, Y. Lu, O. Abu-Qamar, L. P. Aiello, and J. K. Sun, "Estimation of diabetic retinal microaneurysm perfusion parameters based on computational fluid dynamics modeling of adaptive optics scanning laser ophthalmoscopy," Frontiers in Physiology **9**, 989 (2018).

[54]M. Sato and N. Ohshima, "Effect of wall shear rate on thrombogenesis in microvessels of the rat mesentery," Microvascular Research **66**, 941–949 (1990).

[55]J. Zilberman-Rudenko, J. L. Sylman, H. H. S. Lakshmanan, O. J. T. McCarty, and J. Maddala, "Dynamics of blood flow and thrombus formation in a multi-bypass microfluidic ladder network," Cellular and Molecular Bioengineering **10**, 16–29 (2017).

[56]W.-T. Wu, N. Aubry, M. Massoudi, and J. F. Antaki, "Transport of platelets induced by red blood cells based on mixture theory," International Journal of Engineering Science **118**, 16 – 27 (2017).

[57]L. Mountrakis, E. Lorenz, O. Malaspinas, S. Alowayyed, B. Chopard, and A. G. Hoekstra, "Parallel performance of an ib-lbm suspension simulation framework," Journal of Computational Science **9**, 45–50 (2015).

[58]A. M. Robertson, A. Sequeira, and R. G. Owens, "Rheological models for blood," in *Cardiovascular mathematics* (Springer, 2009) pp. 211–241.

[59]A. Celi, G. Merrill-Skoloff, P. Gross, S. Falati, D. S. Sim, R. Flaumen-

AIP Publishing Physics of Fluids ACCEPTED MANUSCRIPT
This is the author's peer reviewed, accepted manuscript. However, the online version of record will be different from this version once it has been copyedited and typeset.
PLEASE CITE THIS ARTICLE AS DOI: 10.1063/5.0216196

haft, B. Furie, and B. Furie, "Thrombus formation: direct real-time observation and digital analysis of thrombus assembly in a living mouse by confocal and widefield intravital microscope," Journal of Thrombosis and Haemostasis **1**, 60–68 (2002).
[60]J. W. Weisel and R. I. Litvinov, "Red blood cells: the forgotten player in hemostasis and thrombosis," Journal of Thrombosis and Haemostasis **17**, 271–282 (2019), https://onlinelibrary.wiley.com/doi/pdf/10.1111/jth.14360.
[61]J. R. Byrnes and A. S. Wolberg, "Red blood cells in thrombosis," Blood **130**, 1795–1799 (2017).
[62]R. I. Litvinov and J. W. Weisel, "Role of red blood cells in haemostasis and thrombosis," ISBT Science Series **12**, 176–183 (2017).
[63]C. Klatt, I. Krüger, S. Zey, K.-J. Krott, M. Spelleken, N. S. Gowert, A. Oberhuber, L. Pfaff, W. Luckstadt, K. Jurk, M. Schaller, H. Al-Hasani, J. Schrader, S. Massberg, K. Stark, H. Schelzig, M. Kelm, and M. Elvers, "Platelet-rbc interaction mediated by fasl/fasr induces procoagulant activity important for thrombosis," The Journal of Clinical Investigation **128** (2018), 10.1172/JCI92077.
[64]E. Kenne, K. F. Nickel, A. T. Long, T. A. Fuchs, E. X. Stavrou, F. R. Stahl, and T. Renné, "Factor XII: a novel target for safe prevention of thrombosis and inflammation," Journal of Internal Medicine **278**, 571–585 (2015).
[65]J. W. Yau, H. Teoh, and S. Verma, "Endothelial cell control of thrombosis," BMC Cardiovascular Disorders **15** (2015), 10.1186/s12872-015-0124-z.
[66]V. W. M. van Hinsbergh, "Endothelium—role in regulation of coagulation and inflammation," Seminars in Immunopathology **34**, 93–106 (2011).
[67]K. Urschel, M. Tauchi, S. Achenbach, and B. Dietel, "Investigation of wall shear stress in cardiovascular research and in clinical practice—from bench to bedside," International Journal of Molecular Sciences **22**, 5635 (2021).
[68]A. M. Malek, "Hemodynamic shear stress and its role in atherosclerosis," JAMA **282**, 2035 (1999).
[69]A. Bouchnita, K. Terekhov, P. Nony, Y. Vassilevski, and V. Volpert, "A mathematical model to quantify the effects of platelet count, shear rate, and injury size on the initiation of blood coagulation under venous flow conditions," PloS one **15**, e0235392 (2020).
[70]A. Bouchnita and V. Volpert, "A multiscale model of platelet-fibrin thrombus growth in the flow," Computers & Fluids **184**, 10–20 (2019).
[71]A. Bouchnita and V. Volpert, "Intraplatelet calcium signaling regulates thrombus growth under flow: Insights from a multiscale model," Computation **12**, 99 (2024).
[72]A. Belyaev, J. Dunster, J. Gibbins, M. Panteleev, and V. Volpert, "Modelling thrombosis in silico: frontiers, challenges, unresolved problems and milestones," Physics of Life Reviews **26–27**, 57–95 (2018).
[73]B. M. Fanni, K. Capellini, M. D. Leonardo, A. Clemente, E. Cerone, S. Berti, and S. Celi, "Correlation between LAA morphological features and computational fluid dynamics analysis for non-valvular atrial fibrillation patients," Applied Sciences **10**, 1448 (2020).
[74]G. Musotto, A. Monteleone, D. Vella, S. D. Leonardo, A. Viola, G. Pitarresi, B. Zuccarello, A. Pantano, A. Cook, G. M. Bosi, and G. Burriesci, "The role of patient-specific morphological features of the left atrial appendage on the thromboembolic risk under atrial fibrillation," Frontiers in Cardiovascular Medicine **9** (2022), 10.3389/fcvm.2022.894187.
[75]M. García-Villalba, L. Rossini, A. Gonzalo, D. Vigneault, P. Martinez-Legazpi, E. Durán, O. Flores, J. Bermejo, E. McVeigh, A. M. Kahn, and J. C. del Álamo, "Demonstration of patient-specific simulations to assess left atrial appendage thrombogenesis risk," Frontiers in Physiology **12** (2021), 10.3389/fphys.2021.596596.
[76]J. Mill, V. Agudelo, A. L. Olivares, M. I. Pons, E. Silva, M. Nuñez-Garcia, X. Morales, D. Arzamendi, X. Freixa, J. Noailly, *et al.*, "Sensitivity analysis of in silico fluid simulations to predict thrombus formation after left atrial appendage occlusion," Mathematics **9**, 2304 (2021).
[77]D. Ram, D. Bhandari, D. Tripathi, and K. Sharma, "Motion of bacteria and caox particles via urine flow modulated by the electro-osmosis," Physics of Fluids **35** (2023).
[78]D. Ram, D. S. Bhandari, K. Sharma, and D. Tripathi, "Progression of blood-borne viruses through bloodstream: A comparative mathematical study," Computer Methods and Programs in Biomedicine **232**, 107425 (2023).
[79]D. Ram, D. Bhandari, D. Tripathi, and K. Sharma, "Propagation of h1n1 virus through saliva movement in oesophagus: a mathematical model," The European Physical Journal Plus **137**, 866 (2022).
[80]C. Inc., "COMSOL Multiphysics," `http://www.comsol.com`.
[81]H. Jasak, A. Jemcov, Z. Tukovic, *et al.*, "Openfoam: A c++ library for complex physics simulations," in *International workshop on coupled methods in numerical dynamics*, Vol. 1000 (IUC Dubrovnik Croatia, 2007) pp. 1–20.
[82]A. Bouchnita, A. Tosenberger, and V. Volpert, "On the regimes of blood coagulation," Applied mathematics letters **51**, 74–79 (2016).
[83]A. Bouchnita, T. Galochkina, and V. Volpert, "Influence of antithrombin on the regimes of blood coagulation: insights from the mathematical model," Acta biotheoretica **64**, 327–342 (2016).
[84]W.-T. Wu, Y. Li, N. Aubry, M. Massoudi, and J. F. Antaki, "Numerical simulation of red blood cell-induced platelet transport in saccular aneurysms," Applied Sciences **7**, 484 (2017).
[85]W.-T. Wu, N. Aubry, J. F. Antaki, and M. Massoudi, "Simulation of blood flow in a sudden expansion channel and a coronary artery," Journal of Computational and Applied Mathematics **376**, 112856 (2020).
[86]`https://www.solidworks.com`.
[87]G. García-Isla, A. L. Olivares, E. Silva, M. Nuñez-Garcia, C. Butakoff, D. Sanchez-Quintana, H. G. Morales, X. Freixa, J. Noailly, T. De Potter, *et al.*, "Sensitivity analysis of geometrical parameters to study haemodynamics and thrombus formation in the left atrial appendage," International journal for numerical methods in biomedical engineering **34**, e3100 (2018).
[88]P. Cignoni, M. Callieri, M. Corsini, M. Dellepiane, F. Ganovelli, and G. Ranzuglia, "Meshlab: an open-source mesh processing tool," in *Eurographics Italian Chapter Conference*, edited by V. Scarano, R. D. Chiara, and U. Erra (The Eurographics Association, 2008).
[89]`https://code-aster.org`.
[90]D. Gisen, "Generation of a 3d mesh using snappyhexmesh featuring anisotropic refinement and near-wall layers," in *ICHE 2014. Proceedings of the 11th International Conference on Hydroscience & Engineering* (2014) pp. 983–990.
[91]L. Marroquin, G. Tirado-Conte, R. Pracoń, W. Streb, H. Gutierrez, G. Boccuzzi, D. Arzamendi-Aizpurua, I. Cruz-González, J. M. Ruiz-Nodar, J.-S. Kim, X. Freixa, J. R. Lopez-Minguez, O. De Backer, R. Ruiz-Salmeron, A. Dominguez, A. McInerney, V. Peral, R. Estevez-Loureiro, E. Fernandez-Nofrerias, A. B. Freitas-Ferraz, F. Saia, Z. Huczek, L. Gheorghe, P. Salinas, M. Demkow, J. R. Delgado-Arana, E. Fernandez Peregrina, Z. Kalarus, A. Elvira Laffond, Y. Jang, J. C. Fernandez Camacho, O.-H. Lee, J. M. Hernández-Garcia, C. Mas-Llado, B. Caneiro Queija, I. J. Amat-Santos, M. Dabrowski, J. Rodés-Cabau, and L. Nombela Franco, "Management and outcomes of patients with left atrial appendage thrombus prior to percutaneous closure," Heart **108**, 1098–1106 (2022), https://heart.bmj.com/content/108/14/1098.full.pdf.
[92]J. Mill, J. Harrison, B. Legghe, A. L. Olivares, X. Morales, J. Noailly, X. Iriart, H. Cochet, M. Sermesant, and O. Camara, "In-silico analysis of the influence of pulmonary vein configuration on left atrial haemodynamics and thrombus formation in a large cohort," in *International Conference on Functional Imaging and Modeling of the Heart* (Springer, 2021) pp. 605–616.
[93]R. I. Issa, "Solution of the implicitly discretised fluid flow equations by operator-splitting," Journal of computational physics **62**, 40–65 (1986).
[94]A. Wufsus, N. Macera, and K. Neeves, "The hydraulic permeability of blood clots as a function of fibrin and platelet density," Biophysical journal **104**, 1812–1823 (2013).
[95]S. P. Jackson, "The growing complexity of platelet aggregation," Blood **109**, 5087–5095 (2007).
[96]M. Merten and P. Thiagarajan, "P-selectin expression on platelets determines size and stability of platelet aggregates," Circulation **102**, 1931–1936 (2000).
[97]Y. Chen, L. A. Ju, F. Zhou, J. Liao, L. Xue, Q. P. Su, D. Jin, Y. Yuan, H. Lu, S. P. Jackson, and C. Zhu, "An integrin αIIbβ3 intermediate affinity state mediates biomechanical platelet aggregation," Nature Materials **18**, 760–769 (2019).
[98]O. V. Kim, Z. Xu, E. D. Rosen, and M. S. Alber, "Fibrin networks regulate protein transport during thrombus development," PLoS computational biology **9**, e1003095 (2013).
[99]A. H. Gillespie and A. Doctor, "Red blood cell contribution to hemostasis,"

AIP Publishing Physics of Fluids ACCEPTED MANUSCRIPT
This is the author's peer reviewed, accepted manuscript. However, the online version of record will be different from this version once it has been copyedited and typeset.
PLEASE CITE THIS ARTICLE AS DOI: 10.1063/5.0216196

Frontiers in Pediatrics **9**, 629824 (2021).
[100]D. Y. Nechipurenko, N. Receveur, A. O. Yakimenko, T. O. Shepelyuk, A. A. Yakusheva, R. R. Kerimov, S. I. Obydennyy, A. Eckly, C. Léon, C. Gachet, E. L. Grishchuk, F. I. Ataullakhanov, P. H. Mangin, and M. A. Panteleev, "Clot contraction drives the translocation of procoagulant platelets to thrombus surface," Arteriosclerosis, Thrombosis, and Vascular Biology **39**, 37–47 (2019).
[101]A. Bouchnita, P. Miossec, A. Tosenberger, and V. Volpert, "Modeling of the effects of il-17 and tnf-α on endothelial cells and thrombus growth," Comptes rendus biologies **340**, 456–473 (2017).
[102]Y. V. Krasotkina, E. I. Sinauridze, and F. I. Ataullakhanov, "Spatiotemporal dynamics of fibrin formation and spreading of active thrombin entering non-recalcified plasma by diffusion," Biochimica et Biophysica Acta (BBA)-General Subjects **1474**, 337–345 (2000).
[103]T. Galochkina, A. Bouchnita, P. Kurbatova, and V. Volpert, "Reaction-diffusion waves of blood coagulation," Mathematical biosciences **288**, 130–139 (2017).
[104]F. Shen, C. J. Kastrup, Y. Liu, and R. F. Ismagilov, "Threshold response of initiation of blood coagulation by tissue factor in patterned microfluidic capillaries is controlled by shear rate," Arteriosclerosis, thrombosis, and vascular biology **28**, 2035–2041 (2008).
[105]J. O. Taylor, K. P. Witmer, T. Neuberger, B. A. Craven, R. S. Meyer, S. Deutsch, and K. B. Manning, "In vitro quantification of time dependent thrombus size using magnetic resonance imaging and computational simulations of thrombus surface shear stresses," Journal of biomechanical engineering **136**, 071012 (2014).
[106]C. Min and W. Tao, "An under-relaxation factor control method for accelerating the iteration convergence of flow field simulation," Engineering Computations **24**, 793–813 (2007).
[107]L. Chen, C. Xu, W. Chen, and C. Zhang, "Left atrial appendage orifice area and morphology is closely associated with flow velocity in patients with nonvalvular atrial fibrillation," BMC Cardiovascular Disorders **21** (2021), 10.1186/s12872-021-02242-9.
[108]J. M. Lee, J. Shim, J.-S. Uhm, Y. J. Kim, H.-J. Lee, H.-N. Pak, M.-H. Lee, and B. Joung, "Impact of increased orifice size and decreased flow velocity of left atrial appendage on stroke in nonvalvular atrial fibrillation," The American Journal of Cardiology **113**, 963–969 (2014).
[109]S. K. Brækkan, E. B. Mathiesen, I. Njølstad, T. Wilsgaard, and J.-B. Hansen, "Hematocrit and risk of venous thromboembolism in a general population. the tromsø study," haematologica **95**, 270 (2010).
[110]A. J. Schreijer, P. H. Reitsma, and S. C. Cannegieter, "High hematocrit as a risk factor for venous thrombosis. cause or innocent bystander?" Haematologica **95**, 182 (2010).
[111]J. Yang, Z. Bai, C. Song, H. Ding, M. Chen, J. Sun, and X. Liu, "Research on the internal flow field of left atrial appendage and stroke risk assessment with different blood models," Bioengineering **10**, 944 (2023).
[112]L. Alinezhad, F. Ghalichi, M. Ahmadlouydarab, and M. Chenaghlou, "Left atrial appendage shape impacts on the left atrial flow hemodynamics: A numerical hypothesis generating study on two cases," Computer Methods and Programs in Biomedicine **213**, 106506 (2022).
[113]S. W. Schneider, S. Nuschele, A. Wixforth, C. Gorzelanny, A. Alexander-Katz, R. R. Netz, and M. F. Schneider, "Shear-induced unfolding triggers adhesion of von willebrand factor fibers," Proceedings of the National Academy of Sciences **104**, 7899–7903 (2007).
[114]M. Zhussupbekov, R. M. Rojano, W.-T. Wu, and J. F. Antaki, "von willebrand factor unfolding mediates platelet deposition in a model of high-shear thrombosis," Biophysical Journal **121**, 4033–4047 (2022).
[115]A. V. Belyaev and Y. K. Kushchenko, "Biomechanical activation of blood platelets via adhesion to von willebrand factor studied with mesoscopic simulations," Biomechanics and Modeling in Mechanobiology (2023), 10.1007/s10237-022-01681-3.
[116]R. M. Rojano, A. Lai, M. Zhussupbekov, G. W. Burgreen, K. Cook, and J. F. Antaki, "A fibrin enhanced thrombosis model for medical devices operating at low shear regimes or large surface areas," PLOS Computational Biology **18**, e1010277 (2022).
[117]K. Kumagai, M. Fukuchi, J. Ohta, S. Baba, K. Oda, H. Akimoto, Y. Kagaya, J. Watanabe, K. Tabayashi, and K. Shirato, "Expression of the von willebrand factor in atrial endocardium is increased in atrial fibrillation depending on the extent of structural remodeling," Circulation Journal **68**, 321–327 (2004).
[118]W. E. Wysokinski, R. M. Melduni, N. M. Ammash, D. T. Vlazny, E. Konik, R. A. Saadiq, I. Gosk-Bierska, J. Slusser, D. Grill, and R. D. McBane, "Von willebrand factor and ADAMTS13 as predictors of adverse outcomes in patients with nonvalvular atrial fibrillation," CJC Open **3**, 318–326 (2021).
[119]D. Hernández-Romero, Á. Lahoz, V. Roldan, E. Jover, A. I. Romero-Aniorte, C. M. Martinez, R. Jara-Rubio, J. M. Arribas, A. Garcia-Alberola, S. Cánovas, M. Valdés, and F. Marín, "Von willebrand factor is associated with atrial fibrillation development in ischaemic patients after cardiac surgery," Europace **18**, 1328–1334 (2015).
[120]M. Fukuchi, J. Watanabe, K. Kumagai, Y. Katori, S. Baba, K. Fukuda, T. Yagi, A. Iguchi, H. Yokoyama, M. Miura, Y. Kagaya, S. Sato, K. Tabayashi, and K. Shirato, "Increased von willebrand factor in the endocardium as a local predisposing factor for thrombogenesis in overloaded human atrial appendage," Journal of the American College of Cardiology **37**, 1436–1442 (2001).
[121]M. Nishimura, T. Hashimoto, H. Kobayashi, T. Fukuda, K. Okino, N. Yamamoto, N. Iwamoto, N. Nakamura, T. Yoshikawa, and T. Ono, "The high incidence of left atrial appendage thrombosis in patients on maintenance haemodialysis," Nephrology Dialysis Transplantation **18**, 2339–2347 (2003).
[122]J. Mill, H. Montoliu, A. H. Moustafa, A. L. Olivares, C. Albors, A. M. Aguado, E. Medina, M. Ceresa, X. Freixa, D. Arzamendi, *et al.*, "Domain expert evaluation of advanced visual computing solutions and 3d printing for the planning of the left atrial appendage occluder interventions," International journal of bioprinting **9** (2023).
[123]T. Stomaci, F. Buonamici, G. Gelati, F. Meucci, and M. Carfagni, "3d-printed models for left atrial appendage occlusion planning: a detailed workflow," Rapid Prototyping Journal **29**, 74–81 (2023).
[124]O. Goitein, N. Fink, V. Guetta, R. Beinart, Y. Brodov, E. Konen, D. Goitein, E. Di Segni, A. Grupper, and M. Glikson, "Printed mdct 3d models for prediction of left atrial appendage (laa) occluder device size: a feasibility study." EuroIntervention: Journal of EuroPCR in Collaboration with the Working Group on Interventional Cardiology of the European Society of Cardiology **13**, e1076–e1079 (2017).
[125]O. De Backer, X. Iriart, J. Kefer, J. E. Nielsen-Kudsk, A. Aminian, L. Rosseel, K. F. Kofoed, J. Odenstedt, S. Berti, J. Saw, *et al.*, "Impact of computational modeling on transcatheter left atrial appendage closure efficiency and outcomes," Cardiovascular Interventions **16**, 655–666 (2023).
[126]J. O. Taylor, K. P. Witmer, T. Neuberger, B. A. Craven, R. S. Meyer, S. Deutsch, and K. B. Manning, "In vitro quantification of time dependent thrombus size using magnetic resonance imaging and computational simulations of thrombus surface shear stresses," Journal of biomechanical engineering **136** (2014).
[127]L. Yang, T. Neuberger, and K. B. Manning, "In vitro real-time magnetic resonance imaging for quantification of thrombosis," Magnetic Resonance Materials in Physics, Biology and Medicine , 1–11 (2020).